doi:10.1093/brain/aww036 BRAIN 2016: 139; 1587–1604 | 1587

BRAIN
A JOURNAL OF NEUROLOGY

A subcutaneous cellular implant for passive immunization against amyloid-β reduces brain amyloid and tau pathologies

Aurélien Lathuilière,[1] Vanessa Laversenne,[1] Alberto Astolfo,[2] Erhard Kopetzki,[3] Helmut Jacobsen,[4] Marco Stampanoni,[2] Bernd Bohrmann,[4] Bernard L. Schneider[1,*] and Patrick Aebischer[1,*]

*These authors contributed equally to this work.

Passive immunization against misfolded toxic proteins is a promising approach to treat neurodegenerative disorders. For effective immunotherapy against Alzheimer's disease, recent clinical data indicate that monoclonal antibodies directed against the amyloid-β peptide should be administered before the onset of symptoms associated with irreversible brain damage. It is therefore critical to develop technologies for continuous antibody delivery applicable to disease prevention. Here, we addressed this question using a bioactive cellular implant to deliver recombinant anti-amyloid-β antibodies in the subcutaneous tissue. An encapsulating device permeable to macromolecules supports the long-term survival of myogenic cells over more than 10 months in immunocompetent allogeneic recipients. The encapsulated cells are genetically engineered to secrete high levels of anti-amyloid-β antibodies. Peripheral implantation leads to continuous antibody delivery to reach plasma levels that exceed 50 μg/ml. In a proof-of-concept study, we show that the recombinant antibodies produced by this system penetrate the brain and bind amyloid plaques in two mouse models of the Alzheimer's pathology. When encapsulated cells are implanted before the onset of amyloid plaque deposition in TauPS2APP mice, chronic exposure to anti-amyloid-β antibodies dramatically reduces amyloid-β_{40} and amyloid-β_{42} levels in the brain, decreases amyloid plaque burden, and most notably, prevents phospho-tau pathology in the hippocampus. These results support the use of encapsulated cell implants for passive immunotherapy against the misfolded proteins, which accumulate in Alzheimer's disease and other neurodegenerative disorders.

1 Neurodegenerative Studies Laboratory, Brain Mind Institute, Ecole Polytechnique Fédérale de Lausanne (EPFL), CH-1015 Lausanne, Switzerland
2 Swiss Light Source, Paul Scherrer Institute (PSI), 5232, Villigen-PSI, Switzerland
3 Pharma Research and Early Development, DTA Neuroscience, Roche Innovation Center Penzberg, F. Hoffmann-La Roche, Switzerland
4 Pharma Research and Early Development, DTA Neuroscience, Roche Innovation Center Basel, F. Hoffmann-La Roche, Switzerland

Correspondence to: Patrick Aebischer,
EPFL-SV-BMI-LEN,
Station 19,
1015 Lausanne,
Switzerland
E-mail: patrick.aebischer@epfl.ch

Correspondence may also be addressed to: Bernard Schneider, EPFL-SV-BMI-LEN, Station 19, 1015 Lausanne, Switzerland
E-mail: bernard.schneider@epfl.ch

Received November 04, 2015. Revised January 06, 2016. Accepted January 19, 2016. Advance Access publication March 8, 2016

Bernd Bohrmann,
Roche Innovation Center Basel,
Grenzacherstrasse 124,
4070 Basel,
F. Hoffmann-La Roche,
Switzerland
E-mail: bernd.bohrmann@roche.com

Keywords: Alzheimer's disease; immunization; encapsulation; cellular implant; antibody

Abbreviations: ECT = encapsulated cell technology; mAb = monoclonal antibody

Introduction

Passive immunization using monoclonal antibodies has recently emerged for the treatment of neurological diseases. In particular, monoclonal antibodies can be administered to target the misfolded proteins that progressively aggregate and propagate in the CNS and contribute to the histopathological signature of neurodegenerative diseases. Alzheimer's disease is the most prevalent proteinopathy, characterized by the deposition of amyloid plaques and neurofibrillary tangles. According to the 'amyloid cascade hypothesis', which is supported by strong genetic evidence (Goate and Hardy, 2012), the primary pathogenic event in Alzheimer's disease is the accumulation and aggregation of amyloid-β into insoluble extracellular plaques in addition to cerebral amyloid angiopathy (Hardy and Selkoe, 2002). High levels of amyloid-β may cause a cascade of deleterious events, including neurofibrillary tangle formation, neuronal dysfunction and death. Anti-amyloid-β antibodies have been developed to interfere with the amyloid-β cascade. Promising data obtained in preclinical studies have validated immunotherapy against Alzheimer's disease, prompting a series of clinical trials (Bard *et al.*, 2000; Bacskai *et al.*, 2002; Oddo *et al.*, 2004; Wilcock *et al.*, 2004*a*; Bohrmann *et al.*, 2012). Phase III trials using monoclonal antibodies directed against soluble amyloid-β (bapineuzumab and solanezumab) in patients with mild-to-moderate Alzheimer's disease showed some effects on biomarkers that are indicative of target engagement. These trials, however, missed the primary endpoints, and it is therefore believed that anti-amyloid-β immunotherapy should be administered at the early presymptomatic stage (secondary prevention) to better potentiate therapeutic effects (Doody *et al.*, 2014; Salloway *et al.*, 2014). For the treatment of Alzheimer's disease, it is likely that long-term treatment using a high dose of monoclonal antibody will be required. However, bolus administration of anti-amyloid-β antibodies may aggravate dose-dependent adverse effects such as amyloid-related imaging abnormalities (ARIA) (Sperling *et al.*, 2012). In addition, the cost of recombinant antibody production and medical burden associated with repeated subcutaneous or intravenous bolus injections may represent significant constraints, especially in the case of preventive immunotherapy initiated years before the onset of clinical symptoms in patients predisposed to develop Alzheimer's disease.

Therefore, alternative methods need to be developed for the continuous, long-term administration of antibodies. Here, we used an implant based on a high-capacity encapsulated cell technology (ECT) (Lathuiliere *et al.*, 2014*b*). The ECT device contains myogenic cells genetically engineered for antibody production. Macromolecules can be exchanged between the implanted cells and the host tissue through a permeable polymer membrane. As the membrane shields the implanted cells from immune rejection in allogeneic conditions, it is possible to use a single donor cell source for multiple recipients. We demonstrate that anti-amyloid immunotherapy using an ECT device implanted in the subcutaneous tissue can achieve therapeutic effects inside the brain. Chronic exposure to anti-amyloid-β monoclonal antibodies produced *in vivo* using the ECT technology leads to a significant reduction of the amyloid brain pathology in two mouse models of Alzheimer's disease.

Materials and methods

Macroencapsulation device

The flat sheet macroencapsulation device was specifically designed for the subcutaneous implantation of cells and was engineered as described elsewhere (Lathuiliere *et al.*, 2014*b*). To guarantee the quality and reproducibility of the device assembly, a process based on ultrasonic welding was implemented. The tight sealing of each device was controlled using an air-leak test. The assembled device was 27-mm long, 12-mm wide and 1.2-mm thick. The distance between the two permeable membranes was between 100 and 300 μm and defined the volume of the inner chamber. A loading port was integrated into the device frame to allow the injection of cells through a 1 ml pipette tip connected to the device. The devices were gas sterilized with ethylene oxide before further use.

MAb-11 monoclonal anti-amyloid-β antibody

MAb-11 is an anti-amyloid-β monoclonal antibody that carries 11 amino acid substitutions compared to gantenerumab (Bohrmann *et al.*, 2012). MAb-11 binds to amyloid-β

aggregates via a conformational epitope with binding properties that are similar to gantenerumab, as demonstrated by equilibrium dissociation constant (K_D) values of 0.14–0.67 nM, which were determined for amyloid-β_{40} and amyloid-β_{42} by surface plasmon resonance (Biacore). MAb-11 was derived from the MorphoSys HuCAL-Fab1 phage display library (Rauchenberger *et al.*, 2003). For the present study, we synthetized two cDNAs, encoding the light and heavy chains of a chimeric version of mAb-11, containing the mouse constant domains of murine IgG2a and the human variable domains of mAb-11. We also used similar chimeric constructs encoding the Fab and F(ab')$_2$ fragments derived from mAb-11 IgG2a and lacking the murine Fc effector domain.

Cell culture and genetic engineering

Cell lines were purchased from the American Type Culture Collection (ATCC) and maintained at 37 °C and 5% CO_2 in medium containing penicillin (100 U/ml) and streptomycin (100 U/ml) (Invitrogen) according to ATCC guidelines. The spontaneously immortalized C8-B4 mouse microglial cell line (ATCC number CRL-2540) (Alliot *et al.*, 1996) was cultured in Dulbecco's modified Eagle medium (DMEM) containing 10% foetal bovine serum (FBS). The C2C12 mouse myoblast cell line (ATCC number CRL-1772), which is derived from the leg skeletal muscles of an adult C3H (H2k) mouse (Yaffe and Saxel, 1977), was grown in similar conditions.

To induce the secretion of the chimeric recombinant mAb-11 IgG2a, C2C12 myoblasts were genetically engineered using a dual lentiviral vector system, as described previously (Lathuiliere *et al.*, 2014*a*). Briefly, cDNAs encoding either the mAb-11 IgG2a light chain or heavy chain were subcloned into the pRRLSIN.cPPT.PGK-GFP.WPRE lentiviral shuttle plasmid (Addgene plasmid #12252). Lentivirus particles were produced using a third-generation system using transient transfection of HEK293T cells with pCMV-dR8.2Δvpr, pMD2.G, pRSV-Rev and the shuttle plasmid (Zufferey, 2002). Viral titres (infectious particles) were determined for each vector by infecting HeLa cells and measuring the number of integrated vector genomes per cell by quantitative polymerase chain reaction (as described in Charrier *et al.*, 2005). A cell population stably expressing mAb-11 was generated by lentiviral transduction of C2C12 myoblasts at a multiplicity of infection (MOI) of 1500 for both the heavy and light chain vectors. From this pool of cells, individual clones were isolated using limiting dilution, expanded and screened according to the measured rate of mAb-11 secretion. For the present study, we used two clonal C2C12 myoblast cell lines, clones #72 and #29, which secrete 13 pg/cell/day and 29 pg/cell/day of the full mAb-11 IgG2a antibody, respectively. In addition, another C2C12 clonal cell line was engineered to produce 11.4 pg/cell/day of a recombinant mAb-11 F(ab')$_2$ fragment (clone #91L). For secretion of the full IgG2a antibody, clone #29 was used in the 5XFAD mouse study and in the second TauPS2APP mouse study. Clone #72 was used in the first TauPS2APP mouse study. For the control ECT devices, capsules were loaded with a population of C2C12 myoblasts transduced with the pRRLSIN.cPPT.PGK-GFP.WPRE lentiviral vector (Addgene plasmid #12252), as described in Lathuiliere *et al.* (2014*a*).

Microglial phagocytosis study

The measurement of antibody-mediated amyloid-β phagocytosis was performed as proposed previously (Webster *et al.*, 2001). In this study, we used either purified preparations of full mAb-11 IgG2a antibody, or a purified Fab antibody fragment. A suspension of 530 μM fluorescent fibrillar amyloid-β_{42} was prepared in 10 mM HEPES (pH 7.4) by stirring overnight at room temperature. The resulting suspension contained 30 μM fluorescein-conjugated amyloid-β_{42} and 500 μM unconjugated amyloid-β_{42} (Bachem). IgG-fibrillar amyloid-β_{42} immune complexes were obtained by preincubating fluorescent fibrillar amyloid-β_{42} at a concentration of 50 μM in phosphate-buffered saline (PBS) with various concentrations of purified mAb-11 IgG2a or Fab antibody fragment for 30 min at 37 °C. The immune complexes were washed twice by centrifugation for 5 min at 14 000*g* and resuspended in the initial volume to obtain a fluorescent fibrillar amyloid-β_{42} solution (total amyloid-β_{42} concentration: 530 μM). The day before the experiment, 8×10^4 C8-B4 cells were plated in 24-well plates. The medium was replaced with serum-free DMEM before the addition of the peptides. The cells were incubated for 30 min with fibrillar amyloid-β_{42} or IgG-fibrillar amyloid-β_{42} added to the culture medium. Next, the cells were washed twice with Hank's Balanced Salt Solution (HBSS) and subsequently detached by trypsinization, which also eliminates surface-bound fibrillar amyloid-β_{42}. The cells were fixed for 10 min in 4% paraformaldehyde and finally resuspended in PBS. The cell fluorescence was determined with a flow cytometer (Accuri C6; BD Biosciences), and the data were analysed using the FlowJo software (TreeStar Inc.). To determine the effect of the anti-amyloid-β antibodies on amyloid-β phagocytosis, the concentration of fluorescent fibrillar amyloid-β_{42} was set at 1.5 μM, which is in the linear region of the dose-response curve depicting fibrillar amyloid-β_{42} phagocytosis in C8-B4 cells (Fig. 2C). All experiments were performed in duplicate.

Transgenic mice

Two different transgenic mouse models were utilized for the present study. The two lines were backcrossed for more than seven generations with C57BL/6N mice. The triple transgenic TauPS2APP mouse line carries transgenes expressing the Swedish (K670N/M671L) mutant of human APP, the N141I mutant of PSEN2 and the P301L mutant of human tau (Grueninger *et al.*, 2010). The 5XFAD mouse line carries two transgenes expressing human APP with three familial mutations [Swedish (K670N/M671L), Florida (I716V) and London (V717I)] and PS1 with two familial mutations (M146L and L286V) (Oakley *et al.*, 2006). The experimental groups were rigorously age-matched. All experiments were performed in accordance with Swiss legislation and with the European Community Council directive (86/609/EEC) for the care and use of laboratory animals. Animals were housed in a controlled temperature room that was maintained in a 12:12 h light:dark cycle and had access to water and food *ad libitum*.

In vivo studies

The devices were loaded with 10^6 mAb-11-expressing C2C12 cells mixed with a hydrogel scaffold composed of 1.5%

polyethylene glycol (PEG) (Ehrbar *et al.*, 2007). Capsules were randomly assigned to individual mice in each group. The detailed procedure for loading and implantation has been previously described (Lathuiliere *et al.*, 2014*b*). Blood was sampled from the facial vein starting at 3 weeks after surgery and then again once every other week until the end of the experiment. The blood was collected in EDTA-coated tubes and centrifuged for 5 min at 1500*g* to separate the plasma. The concentration of mAb-11 was determined by enzyme-linked immunosorbent assay (ELISA) on the same day as collection, and the remaining plasma samples were kept frozen at −80 °C. At the end of the experiment, the animals were sacrificed with an overdose of pentobarbital. Terminal intracardiac puncture was performed to collect the blood samples. The animals were perfused with heparinized PBS. After opening the skull, the brains were carefully dissected and fresh frozen at −80 °C until further use. Implants were dissected from the subcutaneous tissue and incubated overnight in 6-well plates containing DMEM supplemented with 10% FBS. The following day, the mAb-11 secretion level was quantified by incubating the implant in 2.5 ml of fresh culture medium for 1 h. The concentrations of mAb-11 were determined in samples of culture medium by ELISA.

MAb-11 quantification

The mAb-11 concentration was quantified in mouse plasma and culture medium using an ELISA assay, as previously described (Lathuiliere *et al.*, 2014*a*). As standards, we used either purified mAb11 IgG2a or a purified recombinant mAb-11 Fab fragment. The plasma samples were diluted at least 1:100 in Low Cross Buffer (Candor) and loaded in duplicate. The colorimetric reaction was quantified at a wavelength of 405 nm on a Versamax plate reader (Molecular Devices). A standard curve was generated by a non-linear four-parameter fit, and the sample concentration was calculated using SoftMax Pro software (Molecular Devices).

Anti-drug antibody detection assay

To detect antibodies against mAb-11 IgG2a, a direct immunoassay was implemented. Briefly, 96-well microtitre plates were coated with 20 µg/ml of purified mAb-11 and blocked with 2% bovine serum albumin (BSA) in PBS. After incubation with the plasma samples, the presence of bound IgM was measured by incubation with a conjugated goat anti-mouse IgM (Jackson Immunoresearch), followed by a colorimetric reaction with ABTS solution (Roche Applied Science). In a pre-study validation experiment performed with 30 naive plasma samples, the minimal dilution was set to 1:100 and the cut point was determined by calculating the mean plus 1.645 times the standard deviation, corresponding to 5% false positive detection (Geng *et al.*, 2005). For screening, a dynamic cut point was used (Shankar *et al.*, 2008), and the positive samples were serially diluted to determine the anti-drug antibody titre.

Immunohistochemistry

The 10 µm sagittal cryosections were prepared from each mouse brain on Superfrost plus slides (Thermo Scientific). The sections were fixed in −20 °C acetone for 3 min and washed in PBS plus 0.01% Tween-20. For the detection of the mAb-11 IgG2a (plaque immunodecoration), the blocking of non-specific binding sites was performed by incubating the slides in Ultra V blocking solution (LabVision) for 5 min, followed by a wash in PBS plus 0.01% Tween-20 and a subsequent incubation in Power Block solution (BioGenex) with 10% normal sheep serum for 20 min. Cy3-conjugated goat-anti-mouse IgG2a isotype-specific antibody (Jackson Immunoresearch) was diluted to 16 µg/ml in PBS plus 1% BSA and 0.01% Tween-20 and incubated for 1 h at room temperature. For the detection of the $F(ab')_2$ fragment of mAb-11, blocking of endogenous peroxidase was performed using Phenylhydrazine 0.1% in PBS during 1 h at 37 °C. After washing with PBS, brain sections were blocked in 2% NDS, 1% BSA in 0.1% Triton™ X-100 PBS during 2 h at room temperature. Biotin-SP-conjugated goat anti-mouse IgGs recognizing the $F(ab')_2$ fragment (Jackson Immunoresearch) were diluted 1:500 in blocking solution and incubated on slices overnight at 4 °C. For labelling, Alexa Fluor® 568-labelled Tyramide Signal Amplification kit (TSA™, Life technologies) was used according to the manufacturer's instructions. For the detection of amyloid-β plaques, sections were blocked with 2% BSA and 5% normal goat serum in PBS for 1 h at room temperature. Biotinylated 6E10 anti-amyloid-β monoclonal antibody (Covance) was diluted to 1 µg/ml in blocking buffer and incubated overnight at 4 °C. After washing in PBS plus 0.001% Tween-20, an Alexa Fluor® 555 labelled TSA kit was used according to the manufacturer's instructions (Invitrogen). To demonstrate the binding of mAb-11 to amyloid-β plaques, purified mAb-11 at a concentration of 1 µg/ml was incubated overnight at 4 °C on brain sections from the TauPS2APP mice that had not been exposed to any antibody treatment. After three washing steps, the bound mAb-11 antibody was detected with Cy3-conjugated goat anti-mouse IgG2a secondary antibody (Jackson Immunoresearch). Immunodetection of phosphorylated tau with AT8 was performed using the Alexa Fluor® 568-labeled TSA Kit (Life technologies). Biotin-labelled mouse anti-human PHF-Tau monoclonal antibody (AT8, Thermo Scientific) was used at a 1:500 dilution. Immunostaining for phospho-S422 tau was performed as described in (Grueninger *et al.*, 2010). For Iba1 and MC1 immunostainings, mounted sections were fixed for 10 min in 4% paraformaldehyde, washed with PBS and incubated for 1 h at 37 °C in 0.1% phenylhydrazine, followed by blocking in 10% normal goat serum, 1% BSA and 0.3% PBS Triton™ X-100 for 2 h at room temperature. The mouse monoclonal MC1 antibody (provided by P. Davies, 1:500 dilution) and the rabbit anti-Iba1 antibody (Wako, 019-19741, 1:2000 dilution) were incubated with brain sections overnight at 4 °C and revealed with the DAB chromogen. Following Iba1 immunostaining, Congo Red histochemical staining was performed as described in Wilcock *et al.* (2006*b*).

Histological staining

The devices were fixed overnight at 4 °C in 4% paraformaldehyde, dehydrated and processed for embedding in paraffin. Three-micrometre thick sections were prepared on a microtome and stained according to Masson's trichrome protocol. To detect the possible presence of microhaemorrhages in the brain tissue, the Perl's Prussian blue protocol was used to stain the ferric ions present in haemosiderin. An observer blind to

the experimental treatment manually scored the presence of microhaemorrhages on six 25-μm thick sagittal sections chosen at regular intervals across one brain hemisphere of each animal.

Microscopy and image processing

To quantify the amyloid-β plaque load in sections stained with the 6E10 antibody, the slides were scanned using the Virtual Slide System VS120-L100 slide scanner (Olympus) with a 10× objective. For the first two *in vivo* studies, for each mouse, we analysed the presence of amyloid plaques in four sagittal sections, in the medial part of the cortex of one brain hemisphere, with an interval of 100 μm between each section. After manual segmentation of the brain regions of interest, the images were processed by automated thresholding according to Li's minimum cross entropy thresholding method, which is based on an iterative version of the algorithm in ImageJ software. For the last study, for each mouse, we analysed the presence of amyloid plaques in 18 sagittal sections, in the medial part of the cortex of one brain hemisphere, with an inter-slice interval of 60 μm. After manual segmentation of the brain regions of interest, the images were processed by automated thresholding according to Renyi entropy thresholding method.

Representative images of device histology and immunohistological staining of the brain tissue were acquired using a DM 5500 microscope (Leica). For immunodecoration in 5XFAD mouse tissue, high-resolution confocal images were acquired using a 63× NA 1.4 oil immersion objective on a LSM700 Zeiss microscope and deconvoluted with Huygens software (Scientific Volume Imaging). For Immunodecoration on TauPS2APP mice tissue, high-resolution confocal images were acquired using 40× oil immersion objective on a LSM700 Zeiss microscope.

Tau quantification was performed by counting neurons positive for phosphorylated tau (AT8 staining) located in the hippocampal CA1 region (first 600 μm, starting from the subiculum), as described in Collin *et al.* (2014), using an Olympus DP50 microscope equipped with a 10× objective. Six sections located in the medial part of the cortex, with an interslice interval of 60 μm, were counted in each animal.

Microglia quantification was performed by counting Iba1-positive cells within an area of 250 × 250 μm^2 centred on an amyloid plaque stained with Congo Red. If possible, isolated amyloid plaques smaller than 50 μm × 50 μm were preferably considered for the quantification. For control and $F(ab')_2$ treated groups, microglia were counted around two plaques per sections in six sections with an interslice interval of 60 μm. For the IgG2a treated group, considering the very low number of remaining plaques, microglia were counted around 100 plaques distributed as equally as possible among sections and animals. All the quantifications were performed by an observer blind to the experimental groups.

Amyloid-β peptide quantification

The concentration of the amyloid-β_{40} and amyloid-β_{42} peptides was measured using specific commercial ELISA assays (Invitrogen) according to the manufacturer's protocol. Briefly, frozen brain tissue from the lateral part of the cortex was homogenized in 5 M guanidine, 50 mM Tris, pH 8 (at a 1:8 ratio between the wet tissue mass and the buffer mass). Samples were diluted in PBS containing 5% BSA, 0.03% Tween-20 and a complete protease inhibitor cocktail (Roche) before being subjected to the ELISA assay.

Gratings-based X-ray phase contrast tomographic microscopy and quantification of amyloid-β plaques

Whole volume amyloid-β plaque quantifications were performed using grating-based X-ray phase contrast tomographic microscopy as described in Pinzer *et al.* (2012). In brief, the data were collected with a grating interferometer installed at the TOMCAT beamline of the Swiss Light Source with a photon energy of 25 keV (McDonald *et al.*, 2009). The phase grating (pitch of 3.98 μm) and the absorption grating (pitch of 2.00 μm) were placed and aligned at the third Talbot distance (121 mm). A total of 1440 projections were collected over a sample rotation of 180°/7 phase steps of the phase grating. The beam size was 14.6 × 4.2 mm^2 that permitted to scan three half brains at the same time with three vertical scans. The photons were converted in light using a LuAG:Ce scintillator 350-μm thick and subsequently read by a CMOS detector (PCO.Edge) with a pixel size of 6.5 μm. Differential phase contrast slices were reconstructed and filtered accordingly with Pinzer *et al.* (2012). For each sample, a manual segmentation of the brain cortex was done defining our region of interest. The amyloid-β plaques were counted over the region of interest using IDL software (http://www.exelisvis.com) excluding from the result amyloid-β plaques smaller than 10 voxels and larger than 500 voxels (which translate in an equivalent spherical plaque of 17 μm and 64 μm, respectively, in diameter) to avoid the counting of noise signal or artefacts as amyloid-β plaques. The segmentation threshold was carefully decided based on visual investigation on representative samples and kept constant over all the samples. To account for the subjective threshold decision (lower values increase the number of plaques), the counting procedure was run using five different thresholds equally distributed over the initially selected one plus/minus the standard deviation of the background noise [as performed in a similar situation in Astolfo *et al.* (2013)]. The mean (shown in Fig. 7D) and deviation standard calculated over these five total numbers of amyloid-β plaques was used to estimate the plaque density. The number of plaques was determined in individual cubic volumes of 50 × 50 × 50 pixels (50 pixels = 325 μm) and expressed as a density of amyloid-β plaques, colour-coded in Fig. 7B and C.

Statistical analysis

Results were analysed through either one-way or two-way ANOVA, using the Newman-Keuls test for *post hoc* multiple comparisons. For comparisons between two groups, two-tailed heteroscedastic Student's *t*-tests were applied. Correlations were analysed using the Pearson's test. Analyses were performed with the Statistica software (Statsoft). Data are represented as mean ± standard error of the mean (SEM) and the statistical test applied for each dataset is indicated in the

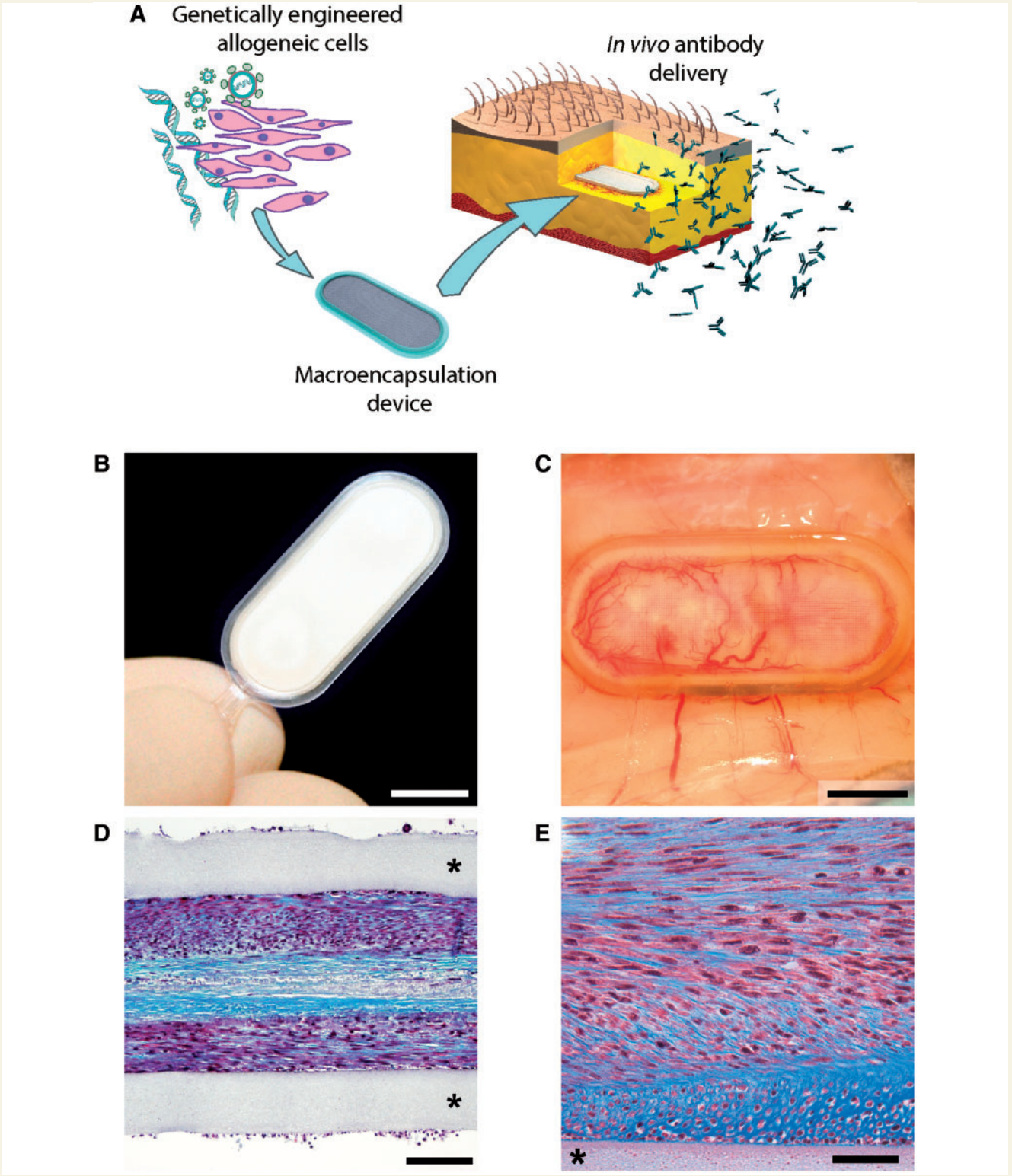

Figure 1 Cell encapsulation device for long-term subcutaneous therapeutic antibody delivery. (**A**) Schematic representation of ECT for passive immunization. Allogeneic cells are genetically engineered using lentiviral vectors to produce a therapeutic antibody. The modified cells are confined in a macroencapsulation 'flat sheet' device and implanted in the subcutaneous tissue for *in vivo* antibody secretion. (**B**) Macroscopic view of the encapsulation device, composed of a transparent frame supporting polymer permeable membranes and reinforced with an outer polyester mesh. (**C**) Dense neovascularization develops around a device containing antibody-secreting C2C12 myoblasts, 8 months after implantation in the mouse subcutaneous tissue. (**D** and **E**) Representative photomicrographs showing encapsulated antibody-secreting C2C12 myoblasts surviving at high density within the flat sheet device 39 weeks after implantation. (**E**) Higher magnification: note that the cells produce a collagen-rich matrix stained in blue with Masson's trichrome protocol. Asterisk: polypropylene porous membrane. Scale bars = 750 μm (**B** and **C**), 100 μm (**D**), 50 μm (**E**).

legend of each figure. The alpha level of significance was set at $P < 0.05$.

Results

Cell encapsulation supports the long-term survival of myoblasts secreting anti-amyloid-β monoclonal antibodies

As an alternative mode for the chronic delivery of therapeutic monoclonal antibodies, we developed a flat sheet ECT device for the subcutaneous implantation of genetically engineered myogenic cells (Fig. 1A) (Lathuiliere *et al.*, 2014*b*). For passive immunization against the amyloid pathology, we genetically modified C2C12 mouse myoblasts using a dual lentiviral vector system to produce a murinized chimeric recombinant IgG2a antibody (mAb-11) directed against both amyloid plaques and amyloid-β oligomers (Lathuiliere *et al.*, 2014*a*). We derived clonal C2C12 cell lines secreting either the full mAb-11 IgG2a antibody, or a recombinant mAb-11 F(ab')$_2$ fragment, which retains the ability to bind amyloid-β but lacks the antibody Fc portion.

The high-capacity flat sheet ECT device developed for subcutaneous implantation was based on a polypropylene frame (1 cm × 2.5 cm) supporting two polypropylene membranes with 0.45 μm pores (Fig. 1B). The device was mechanically reinforced with a polyester mesh apposed on the external face of the porous membrane, which allowed for the development of a dense neovascularization network following implantation in the subcutaneous tissue (Fig. 1C). Prior to device implantation, 10^6 C2C12 myoblasts were mixed with a degradable PEG hydrogel and injected inside the device. After a 9-month implantation in C57BL/6 mice, the C2C12 cells had expanded in the capsule inner space to form a dense cell mass interspersed with a collagen-rich extracellular matrix (Fig. 1D and E). When loaded with mAb-11-secreting myoblasts, this cellular implant was found to continuously produce recombinant anti-amyloid-β antibodies both *in vitro* and *in vivo*.

The plaque-specific mAb-11 antibody enhances fibrillar amyloid-β phagocytosis by microglial cells

We determined *in vitro* if the chimeric recombinant IgG2a mAb-11 was able to bind aggregated amyloid-β and enhance phagocytosis by mouse microglial cells, a mechanism that has been proposed to mediate the clearance of amyloid plaques (Bard *et al.*, 2000; Bohrmann *et al.*, 2012; Demattos *et al.*, 2012). Brain sections from 16-month-old TauPS2APP mice incubated with mAb-11 showed specific binding to brain amyloid deposits (Fig. 2A), consistent with the high affinity of mAb-11 for aggregated amyloid-β. Next, we incubated C8-B4 mouse microglial cells with fluorescent amyloid-β_{42} fibrils, and assessed their ability to internalize fibrillar amyloid-β_{42} by flow cytometry. The cell fluorescence increased as a function of the fibrillar amyloid-β_{42} concentration (Fig. 2B), in a linear relationship at fibrillar amyloid-β_{42} concentrations < 5 μM (Fig. 2C). Internalization of fibrillar amyloid-β_{42} at a concentration of 1.5 μM was significantly increased following preincubation with mAb-11 IgG2a (Fig. 2D). As expected, the increased uptake of fibrillar amyloid-β by microglial cells was mediated by the Fc region, as no effect was found by preincubating fibrillar amyloid-β_{42} with a mAb-11-derived Fab fragment lacking the Fc effector domain ($P = 0.00017$ compared to full IgG2a).

Passive immunization by ECT delivery of mAb-11 decreases amyloid brain pathology in 5XFAD mice

We assessed the efficacy of ECT-mediated immunotherapy in a mouse model of Alzheimer's disease with a rapidly evolving amyloid pathology. 5XFAD mice overexpress mutated forms of the human amyloid precursor protein (APP) and human presenillin 1 (PS1, encoded by *PSEN1*). The induced amyloid-β_{42} production leads to intraneuronal amyloid-β accumulation at 1.5 months and amyloid plaque deposition after only 2 months (Oakley *et al.*, 2006). To model the secondary prevention of Alzheimer's disease, age-matched cohorts of 5XFAD mice were implanted between 5 and 12 weeks of age, after the onset of plaque deposition. Flat sheet devices were loaded with C2C12 myoblasts secreting the full mAb-11 IgG2a (clone #29). Just 7 weeks after implantation, 15.2 ± 3.8 μg/ml of mAb-11 could be detected in the plasma, further increasing to 59.1 ± 6.7 μg/ml at the experimental end-point, 19 weeks post-implantation (Fig. 3A). Explanted devices secreted, on average, 105.5 ± 11.2 μg/day of mAb11 IgG2a (Fig. 3A). Based on the pharmacokinetic parameters measured by injecting recombinant mAb-11 in mice (Supplementary material), the total antibody exposure (3.96 ± 0.43 mg/ml∗day) was estimated to be equivalent to weekly intravenous injections of recombinant mAb-11 IgG2a at a dose of 16.7 ± 1.9 mg/kg for 19 weeks (Supplementary material).

We sought to determine whether the antibodies produced by ECT could be detected inside the brain. Indeed, the blood–brain barrier limits IgG penetration into the brain, with a typical plasma/brain antibody concentration ratio between 100 and 1000 (Wang *et al.*, 2008; Tabrizi *et al.*, 2010). In all mice implanted with a mAb-11 releasing ECT device, brain sections showed antibody immunodecoration localizing to amyloid-β plaques, as indicated by mouse IgG2a immunoreactivity (Fig. 3B). IgG2a

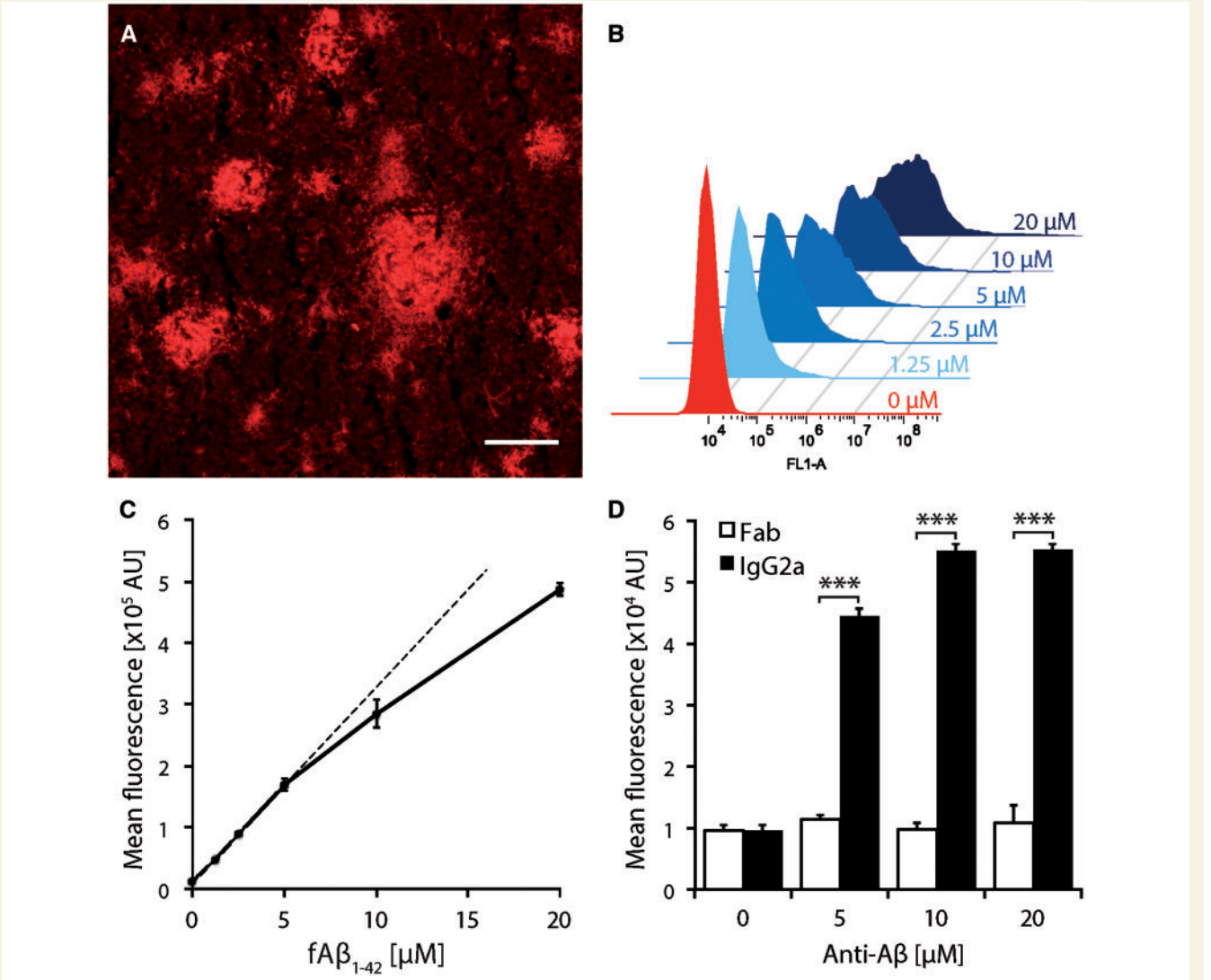

Figure 2 The plaque-specific anti-amyloid-β mAb-11 antibody enhances amyloid phagocytosis by microglial cells. (**A**) Brain section from a 16-month-old TauPS2APP mouse incubated with 1 µg/ml mAb-11 IgG2a antibody. Anti-mouse IgG staining reveals specific binding to diffuse amyloid deposits and the dense cores of amyloid plaques. Scale bar = 50 µm. (**B**) Flow cytometry analysis of C8-B4 microglial cells incubated with increasing concentrations of fluorescent fibrillar amyloid-β_{42} (fAβ_{42}). Histograms of the fluorescence intensity demonstrate the dose-dependent internalization of fibrillar amyloid-β_{42}. (**C**) The mean fluorescence intensity of C8-B4 microglial cells increases as a function of the fibrillar amyloid-β_{42} concentration. Note the linear increase in fluorescence intensity with low fibrillar amyloid-β_{42} concentrations (0–5 µM). Data are expressed as the mean ± SEM; $n = 2$ per condition. (**D**) Preincubation of fluorescent fibrillar amyloid-β_{42} (1.5 µM) with mAb-11 IgG2a enhances internalization in C8-B4 microglial cells. No effect is observed when fibrillar amyloid-β_{42} is pre-incubated with mAb-11 Fab fragments lacking the Fc region. Data are expressed as the mean + SEM; $n = 2$ per condition. Two-way ANOVA with Neuman-Keuls *post hoc* test: $***P < 0.001$; group effect $F(1,14) = 1998.7$, $P = 6.92 \times 10^{-11}$.

immunofluorescence was observed on fibrillar bundles around plaques and on the dense cores of amyloid-β aggregates (Fig. 3C).

To assess the amyloid pathology in 5XFAD mice, we performed anti-amyloid-β immunohistochemistry on brain sections. Dense and widespread amyloidosis, mainly affecting the cortex, hippocampus and thalamus, was found in 5- to 6-month-old animals implanted with devices containing GFP-expressing C2C12 myoblasts (Fig. 4A and B). Amyloid pathology was reduced in the 5XFAD mice treated with the mAb-11 secreting devices (Fig. 4C and D). Quantitative morphometry showed a significant reduction of the percentage of area covered with amyloid-β plaques in the cortex (−31.0%, $P = 0.0069$), hippocampus (−18.1%, $P = 0.018$) and thalamus (−31.7%, $P = 0.013$) (Fig. 4E). Plaque density was decreased in the same brain regions (cortex: −37.8%, $P = 0.00005$; hippocampus: −20.1%, $P = 0.002$; thalamus: −30.3%, $P = 0.007$; Fig. 4F). The median plaque area was significantly increased in the treated mice ($P = 0.012$; Fig. 4G), consistent with a clearance of small amyloid deposits revealed by the shift in the plaque size distribution (Supplementary Fig.

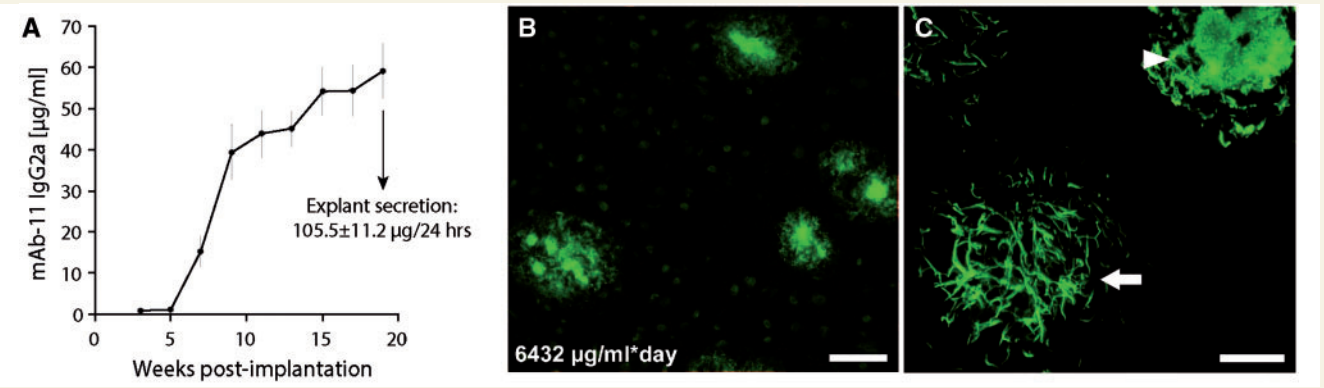

Figure 3 Anti-amyloid-β antibodies delivered by ECT in the subcutaneous tissue bind to amyloid plaques in the brain of 5XFAD mice. (**A**) Plasma levels of mAb-11 in 5XFAD mice implanted for 19 weeks with ECT devices containing mAb-11-secreting C2C12 myoblasts (clone 29, 29 pg mAb-11/cell/day). The bar graph shows the mAb-11 secretion rates of the ECT devices after explantation. Data are expressed as the mean ± SEM; $n = 16$. (**B**) Representative photomicrograph showing mAb-11 immunodecoration (green pseudocoloured IgG2a immunostaining) on amyloid-β plaques in the frontal cortex of a 27-week-old 5XFAD mouse exposed to 6432 µg/ml∗day of antibody in the plasma. (**C**) High magnification confocal imaging of mAb-11 immunodecoration on amyloid-β plaques. Note that mAb-11 binds both fibrillar bundles (arrow) and plaques with a dense amyloid core (arrowhead). Scale bars = 100 µm (**B**), 10 µm (**C**).

1). In cortical homogenates, the mAb-11 treatment significantly reduced the levels of total amyloid-β_{42} ($P = 0.0027$) and amyloid-β_{40} ($P = 0.0025$) (Fig. 4H). We found a significant negative correlation between the total amyloid-β_{42} levels and the exposure to mAb-11 in the plasma, indicating that treatment efficacy primarily depends on the amount of antibody delivered (Fig. 4I). Prussian blue staining did not reveal any sign of microhaemorrhages in the mAb-11-treated mice (data not shown). Because mAb-11 IgG2a comprised complementarity-determining regions (CDR) derived from the human antibody, we tested whether the treated animals developed an anti-drug antibody response by measuring the presence of antibodies recognizing mAb-11 in the mouse plasma. Only 1 of 16 animals developed a significant anti-drug antibody response with the detectable presence of anti-mAb-11 IgM (data not shown). Overall, our results demonstrate that ECT-mediated peripheral immunotherapy can partially oppose amyloid pathology in the rapidly developing 5XFAD mouse model.

Preventive mAb-11 immunization by ECT reduces amyloid pathology in the brain of TauPS2APP mice

Immunization against amyloid-β has been shown to be most effective when initiated before the onset of plaque deposition in mouse models of Alzheimer's disease (Das *et al.*, 2001; Levites *et al.*, 2006). To further assess the effect of passive immunization, we next used TauPS2APP mice, a slowly progressing model that develops both amyloid and tau pathologies, and therefore more closely mimics sporadic Alzheimer's disease. The first experiment is described in the Supplementary material and Supplementary Fig. 2. Briefly, ECT devices secreting mAb-11 IgG2a were implanted in 7-month-old TauPS2APP mice, leading to chronic antibody exposure for 39 weeks. Similarly to the previous experiment in 5XFAD mice, ECT-mediated passive immunization led to a significant decrease in amyloid deposition. However, 7 of 15 mAb-11-treated animals had detectable levels of anti-mAb-11 IgM, indicating that this mouse model may be more prone to develop an anti-drug antibody response potentially neutralizing part of the treatment effects.

In a second experiment, ECT devices were subcutaneously implanted in 2-month-old TauPS2APP mice to deliver mAb-11 antibodies 6 months before the onset of amyloid deposition outside the hippocampus. The mice were transiently injected with anti-CD4 antibodies to block the anti-drug antibody response against mAb-11. Three groups of mice received either control GFP-expressing myoblasts, myoblasts secreting the mAb-11 IgG2a antibody (clone #29), or myoblasts producing a mAb-11-derived F(ab')$_2$ fragment. Already 3 weeks after implantation of the antibody-releasing device, both the full mAb-11 IgG2a (16.2 µg/ml, Fig. 5A) and the mAb-11 F(ab')$_2$ fragment (0.5 µg/ml, Fig. 5B) were detectable in the plasma of the respective groups of mice. Plasma levels then stabilized at ~50 µg/ml (mAb-11 IgG2a) and 2 µg/ml [mAb-11 F(ab')$_2$] until the experimental end-point, 41 weeks after implantation. Explanted devices showed secretion rates reaching on average 33.7 ± 9.7 µg/day for the mAb-11 IgG2a (~150 kDa) and 17.7 ± 2.8 µg/day for the mAb-11 F(ab')$_2$ fragment (~110 kDa). Higher secretion rate, higher stability and longer half-life of the full IgG, compared to the F(ab')$_2$ fragment, all contribute to the 25-fold difference seen in the plasma concentration. Total plasma exposure to mAb-11 IgG2a during the 41-week implantation period (14.8 mg/ml∗day) was estimated to be equivalent to a regimen of weekly intravenous injections at a dose of 29.5 mg/kg.

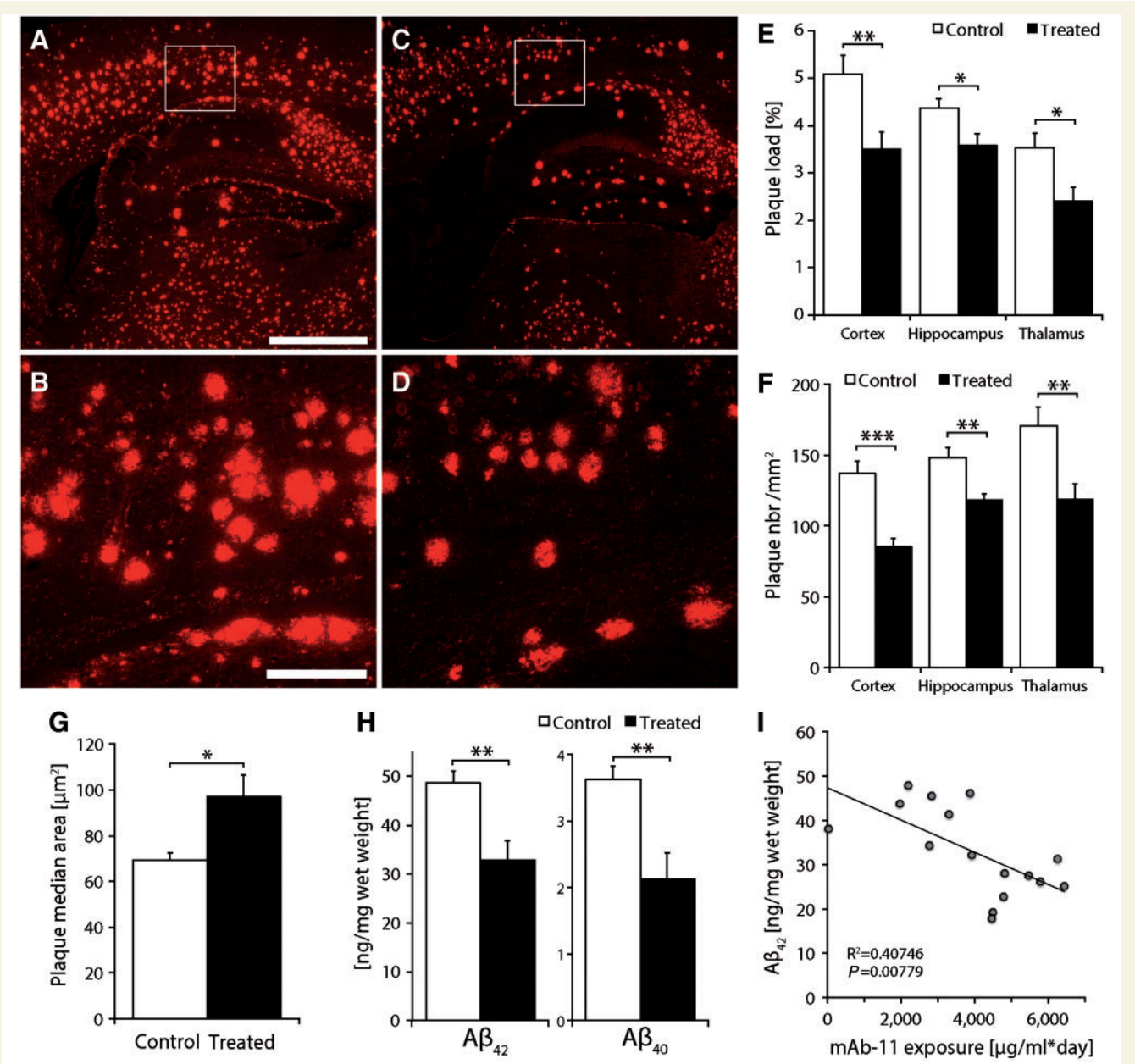

Figure 4 Continuous anti-amyloid-β antibody delivered by ECT reduces amyloid burden in 5XFAD mice. (**A**–**D**) Representative photomicrographs of the amyloid pathology (6E10 immunofluorescence) in 5XFAD mice implanted for 19 weeks with control devices (containing GFP-expressing C2C12 myoblasts) (**A** and **B**) or with devices secreting mAb-11 (**C** and **D**). In these 5- to 6-month-old mice, the staining reveals a robust amyloid pathology that is reduced in the treated animals (**C** and **D**). (**B** and **D**) Higher magnifications of the regions outlined in (**A**) and (**C**), respectively. (**E**) The quantification of amyloid-β burden shows a significant reduction in the plaque load (percentage of the section surface occupied by plaques) in the cortex, hippocampus and thalamus of treated mice. (**F**) The density of amyloid plaques is significantly decreased in these brain regions. (**G**) The median amyloid plaque area is significantly larger in the treated animals. (**H**) The analysis of brain homogenates demonstrates a significant reduction in the amount of amyloid-β_{42} and amyloid-β_{40} peptides in mice implanted with mAb-11-releasing devices. (**I**) The level of amyloid-β_{42} in cortex homogenates is significantly correlated with the total exposure to mAb-11 in the plasma of the treated animals. Data are expressed as the mean + SEM. $n = 15$ per group. Two-tailed heteroscedastic *t*-tests: $^{*}P < 0.05$; $^{**}P < 0.01$; $^{***}P < 0.001$. Correlation is analysed with the Pearson's test. Scale bars = 1 mm (**A**), 200 µm (**C**).

The amyloid pathology was analysed in 1-year-old TauPS2APP mice, 41 weeks after device implantation. The recombinant antibodies produced by ECT were found to immunodecorate amyloid-β plaques in the cortex of the treated mice (Fig. 5C). As expected, detection of mouse IgG F(ab')$_2$ fragments revealed the presence of both the full IgG2a and the F(ab')$_2$ fragment on amyloid plaques in the two groups of treated mice, whereas an Fc region-specific antibody was able to detect plaque immunodecoration only in the IgG2a-treated mice. Next, we

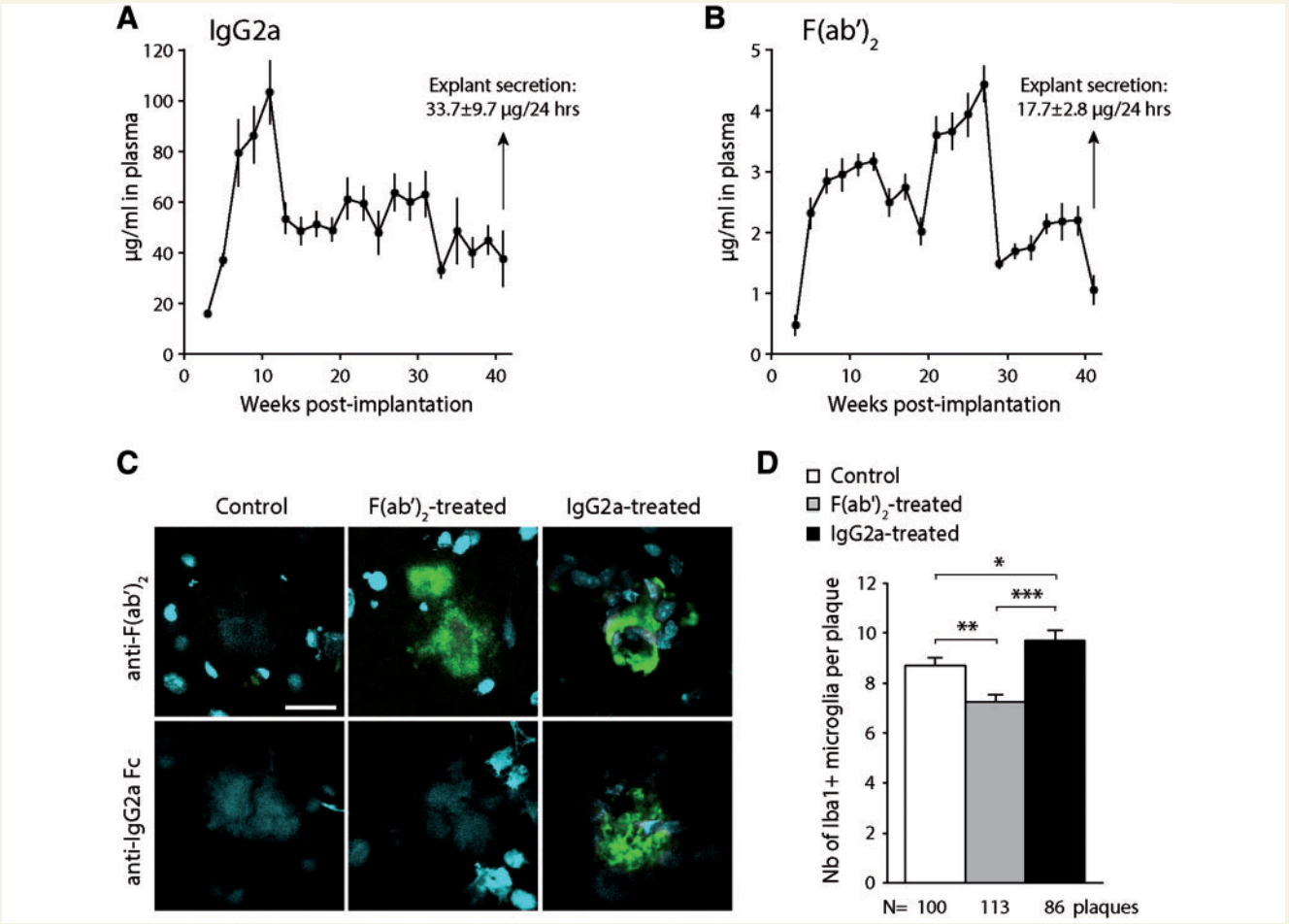

Figure 5 Preventive mAb-11 delivery using ECT affects the local recruitment of microglial cells in TauPS2APP mice. (**A** and **B**) Plasma levels of mAb-11 in TauPS2APP mice implanted for 41 weeks with devices containing either IgG2a-secreting C2C12 myoblasts (**A**), or $F(ab')_2$ fragment-secreting C2C12 myoblasts (**B**). The bar graph shows the mAb-11 secretion rate of the ECT devices after explantation. Data are expressed as the mean ± SEM; $n = 10$. (**C**) Representative photomicrographs showing mAb-11 immunodecoration (green pseudocoloured immunostaining) on amyloid-β plaques in the frontal cortex of a TauPS2APP mice implanted with either control, IgG2a-secreting or $F(ab')_2$-secreting devices. Note that the anti-IgG2a Fc antibody detects only the presence of the full IgG2a antibody, confirming staining specificity. Nuclei are stained with DAPI. (**D**) Quantification of Iba1-positive microglial cells present around amyloid plaques in each group of mice. Note the significant decrease in microglial cell density around plaques in $F(ab')_2$-treated TauPS2APP mice and the increase in IgG2a-treated mice. The number of plaques analysed in each group is indicated. Data are expressed as the mean ± SEM; $F(ab')_2$- and IgG2a-treated groups: $n = 10$. One-way ANOVA with Newman-Keuls *post hoc* test: $^{*}P < 0.05$, $^{**}P < 0.01$, $^{***}P < 0.001$. Scale bar = 20 µm.

assessed if the mAb-11 treatment had any effect on the recruitment of Iba1-positive microglial cells near amyloid deposits (Congo red staining) (Supplementary Fig. 3 and Fig. 5D). In the cortex of control TauPS2APP mice, there were on average 8.7 ± 0.3 Iba1-positive microglial cells neighbouring Congo red-stained individual plaques. The number of microglial cells around plaques was significantly decreased to 7.3 ± 0.3 in the $F(ab')_2$-treated mice, whereas it was increased to 9.7 ± 0.4 in the IgG2a-treated mice. Therefore, the recruitment of microglial cells depends on the presence of the Fc region of the mAb-11 antibody bound to the amyloid plaques.

When initiated before plaque deposition occurred in TauPS2APP mice, the chronic subcutaneous delivery of mAb-11 IgG2a led to a dramatic reduction in amyloid burden detected by anti-amyloid-β immunohistochemistry, compared with the mice implanted with control devices (Fig. 6A). Plaque load was clearly reduced throughout the cortex (−79.9%, $P = 0.004$) and hippocampus (−78.5%, $P = 0.017$) (Fig. 6B). Similarly, the number of plaques was dramatically decreased in both regions (−94.5% and −92.7%, respectively; Fig. 6C). There was minimal deposition of amyloid plaques in the thalamus of 12-month-old TauPS2APP mice. In contrast, the amyloid burden was reduced by only 15–20% with $F(ab')_2$-secreting devices, an effect that was not significant ($P > 0.2$). Compared to the control group, amyloid-β levels were also dramatically reduced in the cortex of IgG2a-treated mice, for both

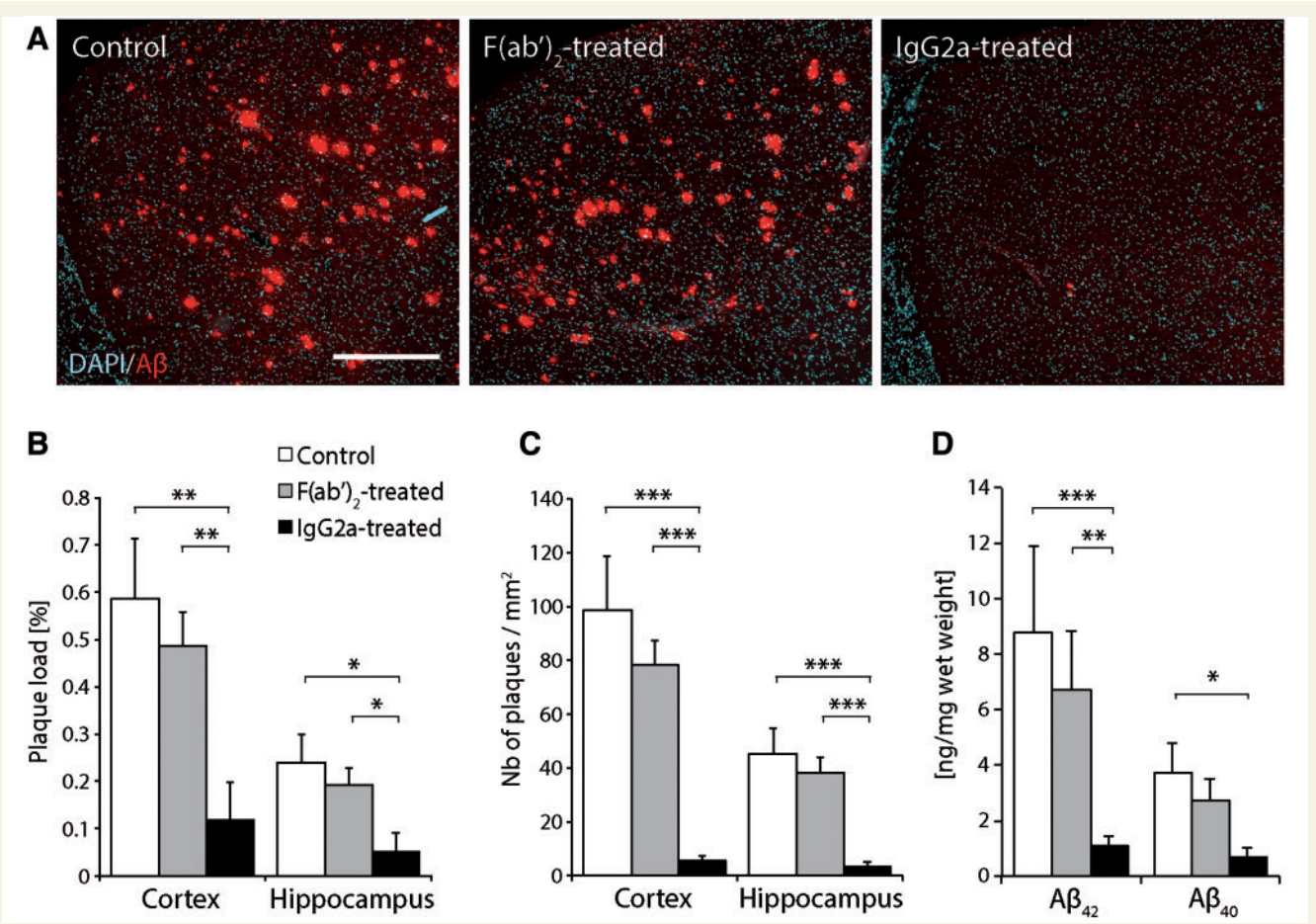

Figure 6 Preventive mAb-11 immunization using ECT delivery strongly reduces amyloid load in the brain of TauPS2APP mice. (**A**) Amyloid burden revealed by anti-amyloid-β immunostaining (6E10) in the frontal cortices of 12-month-old TauPS2APP mice. Note the decreased amyloid pathology in the cortex of the TauPS2APP mouse continuously treated with mAb-11 IgG2a. (**B**) Plaque load, expressed as the percentage of the brain area occupied by amyloid-β-positive plaques, is significantly reduced in the cortex and hippocampus of mice treated with mAb-11 IgG2a. (**C**) The density of amyloid plaques is significantly decreased in these brain regions. (**D**) The amount of amyloid-β_{42} and amyloid-β_{40} is significantly decreased in the cortex of mice treated with mAb-11 IgG2a. Data are expressed as the mean ± SEM; Control group: $n = 8$, $F(ab')_2$- and IgG2a-treated groups: $n = 10$. One-way ANOVA with Newman-Keuls *post hoc* test: $^{*}P < 0.05$, $^{**}P < 0.01$, $^{***}P < 0.001$. Scale bar = 500 μm (**A**).

amyloid-β_{42} (−87.4%, $P = 0.0002$) and amyloid-β_{40} (−82.5%, $P = 0.024$), whereas the effect of the $F(ab')_2$ fragment remained minimal (Fig. 6D). Of note, the level of amyloid-β_{42} in the cortex of 12-month-old TauPS2APP mice was more than 5-fold lower compared to 7-month-old 5XFAD mice (compare Figs 6D and 4H). Altogether, these results indicate that when delivered by ECT, full IgG2a antibodies are more effective than $F(ab')_2$ fragments for the clearing of amyloid pathology, most likely because ECT leads to higher levels of circulating mAb-11 IgG2a in the plasma (Fig. 5A and B).

Strong reduction of plaque density throughout the whole cortex of ECT-mAb-11 treated mice

To further quantify the number of amyloid plaques in ECT-treated mice, the entire contralateral hemicortex of the treated mice was analysed by gratings-based X-ray phase contrast tomographic microscopy (Weitkamp *et al.*, 2005; Pinzer *et al.*, 2012). This technique allows full brain visualization and does not rely on immunodetection methods, which may be subject to interference with the therapeutic antibody bound to amyloid-β. X-ray phase contrast revealed the presence of discrete hyperintense dots throughout the entire cortex of 12-month-old TauPS2APP mice implanted with control devices. These dots were previously shown to correspond to amyloid deposits (Pinzer *et al.*, 2012). The density of plaques in the cortex (plaques/mm^3) was determined following threshold segmentation (Fig. 7A and B and Supplementary Videos 1–3). Coronal maximum-intensity maps show that plaque density was clearly reduced in the entire hemicortex of the mAb-11 IgG2a-treated mice (Fig. 7C). In contrast, the density and distribution of amyloid plaques were similar in

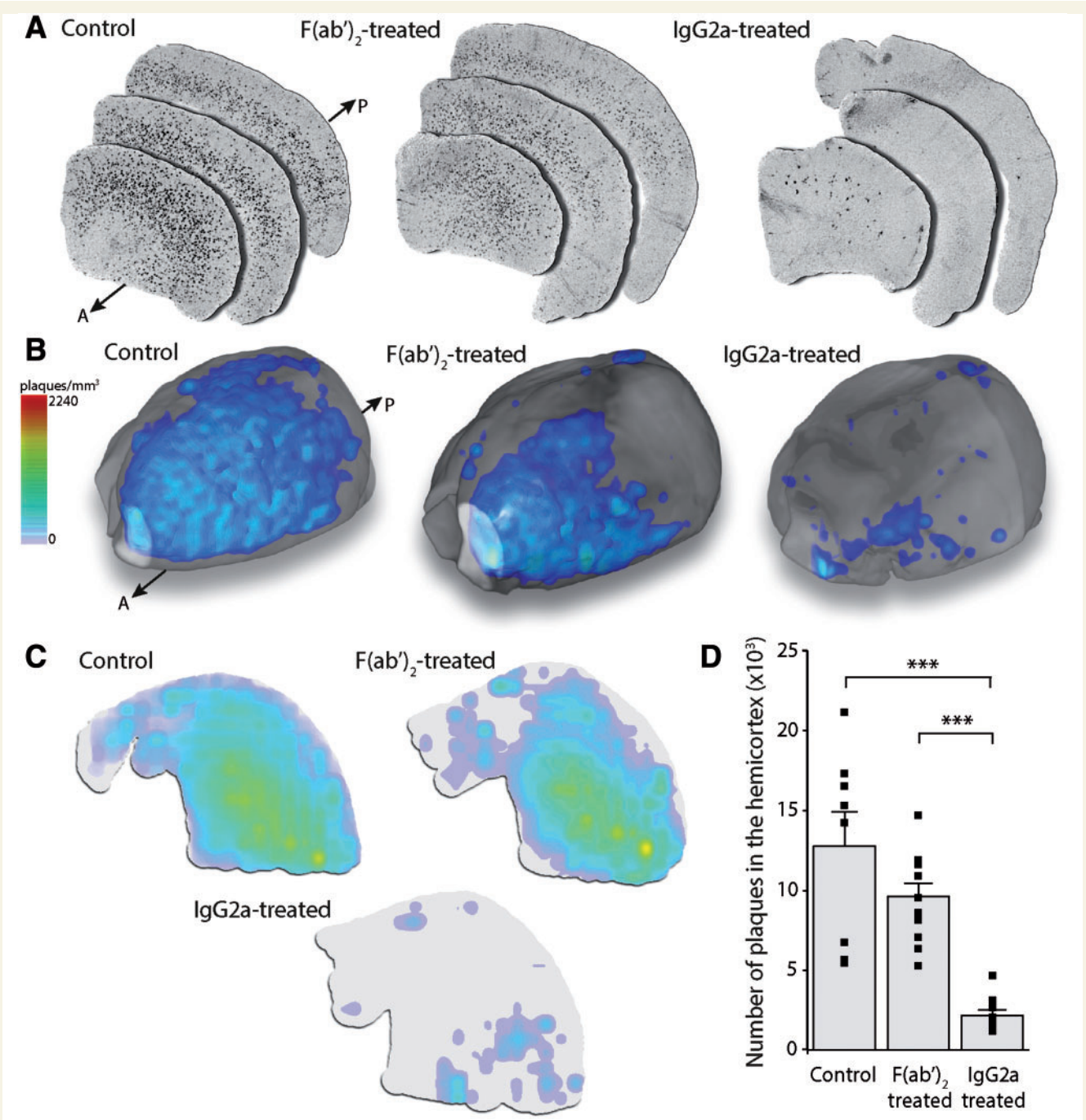

Figure 7 ECT delivery of mAb-11 IgG2a prevents amyloid plaque deposition throughout the entire cortex of TauPS2APP mice. (**A**) Phase-contrast tomographic microscopy of the whole hemicortex reveals hyperintense signals in 12-month-old TauPS2APP mice. The signals are shown on three cortex sections for three representative mice, one from each group, along the anterior (A)–posterior (P) axis. Note the reduction in hyperintense signals in the mAb-11 IgG2a-treated mice. (**B**) Representative hemicortex with superimposed colour-coded density of the hyperintense dots (plaques/mm^3). Note that IgG2a-treated mice have detectable plaques only in the most frontal part of the cortex. (**C**) Coronal maximum-intensity maps of the representative hemicortex. Note the overall reduction in plaque density in the IgG2a-treated mouse. (**D**) Quantification of the total number of plaques in the hemicortex of mice implanted either with control, mAb-11 F(ab')$_2$- and mAb-11 IgG2a-secreting ECT devices. Data are expressed as the mean ± SEM; Control group: $n = 8$, F(ab')$_2$-treated: $n = 11$, IgG2a-treated: $n = 10$. One-way ANOVA with Newman-Keuls *post hoc* test: $^{***}P < 0.001$.

control and F(ab')$_2$-treated mice. Volumetric information from the phase contrast CT datasets was used to determine the total number of plaques in the hemicortex of the mice in each group (Fig. 7D). The mAb-11 IgG2a treatment dramatically reduced the number of detectable plaques (−83%, $P = 0.00013$), whereas the effect of the F(ab')$_2$ treatment was not significant (−25%, $P = 0.0697$).

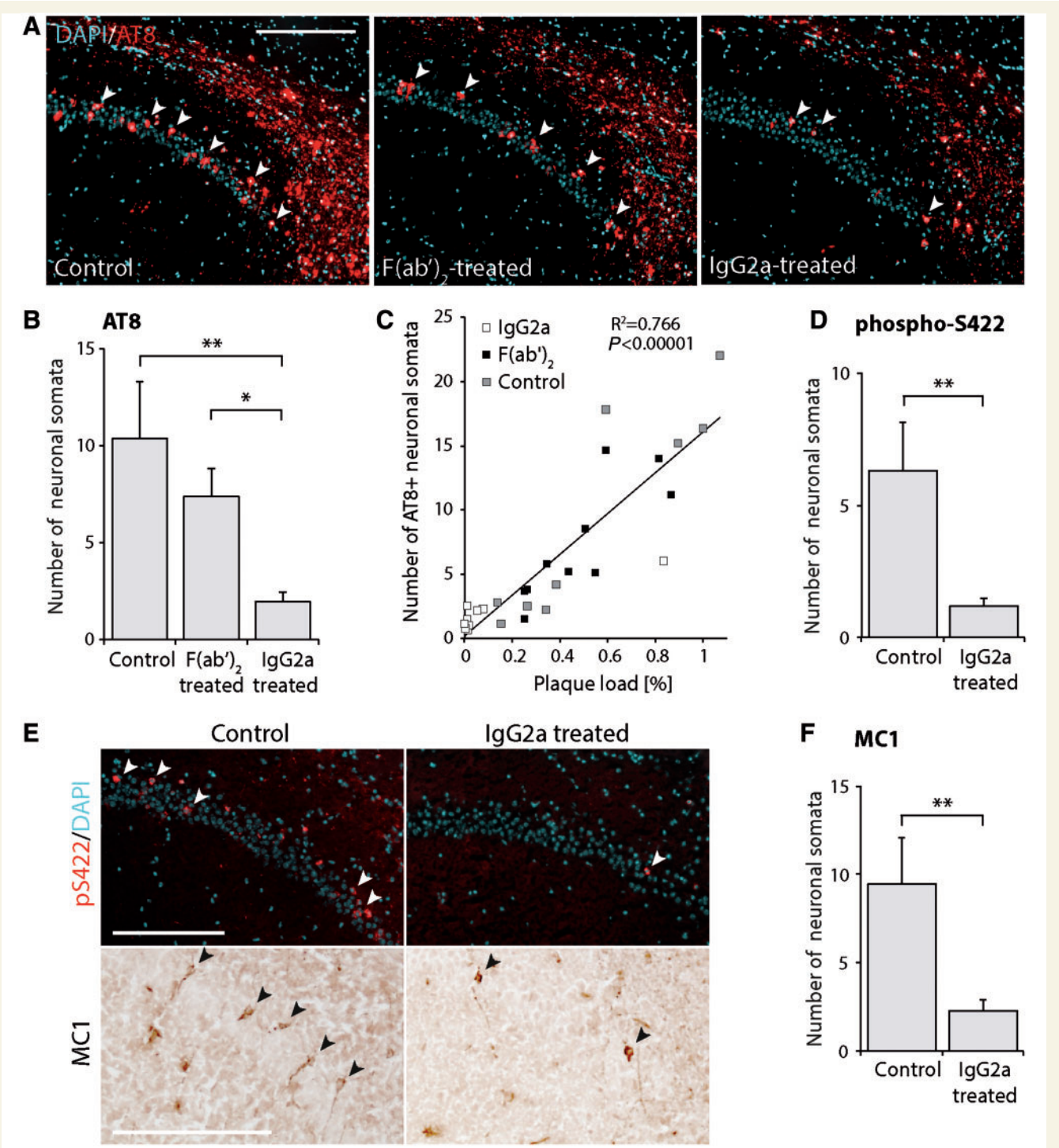

Figure 8 ECT delivery of mAb-11 IgG2a decreases tau pathology in the CA1 region of the hippocampus of TauPS2APP mice. (**A**) Representative photomicrographs of the CA1 region of the hippocampus. Neurons are stained for tau phosphorylated at serine 202 and threonine 205 residues (AT8), and nuclei are stained with DAPI. AT8-positive neuronal somata in the pyramidal layer are indicated with arrowheads. (**B**) Quantification of the number of AT8-positive neurons in the CA1 pyramidal layer of the hippocampus. Note the significant reduction in mAb-11 IgG2a treated mice. (**C**) Correlation between amyloid-β burden and the number of AT8-positive neurons in the CA1 hippocampal region. Individual values from control, mAb-11 F(ab')$_2$-treated and IgG2a-treated mice are shown in the same graph for correlation. (**D**) Quantification of the number of neurons with somatodendritic localization of phospho-S422 tau in the CA1 pyramidal layer of the hippocampus. (**E**) Representative images of phospho-S422 tau and MC1 stainings in the hippocampal CA1 region. Arrowheads indicate neurons with somatodendritic staining. (**F**) Quantification of the number of MC1-positive neuronal somata in the CA1 pyramidal layer. Data are expressed as the mean ± SEM; Control group: $n = 8$, F(ab')$_2$- and IgG2a-treated groups: $n = 10$. One-way ANOVA with Newman-Keuls *post hoc* test (**B**) and two-tailed heteroscedastic *t*-tests (**D** and **F**): $^{*}P < 0.05$, $^{**}P < 0.01$. Correlation in (**C**) is analysed with the Pearson's test. Scale bar = 200 μm (**A** and **E**).

Reduced amyloid-β deposition correlates with decreased tau pathology in the CA1 hippocampus

Next, we analysed the presence of hyperphosphorylated forms of human tau in the CA1 region of the hippocampus of TauPS2APP mice, which overexpress P301L-mutated human tau (Fig. 8A). We assessed the number of neurons located in the CA1 pyramidal layer with an accumulation of AT8-positive phospho-tau (S202/T205) in the somatodendritic compartment (Fig. 8B). In mAb-11 IgG2a-treated mice, the number of AT8-positive neurons was significantly decreased with respect to both control ($P = 0.005$) and F(ab')$_2$-treated mice ($P = 0.035$). However, there was no significant difference between the control and F(ab')$_2$-treated groups ($P = 0.2$). Furthermore, the number of AT8-positive neurons in the CA1 was strongly correlated with amyloid burden in the cortex across all three groups (Fig. 8C), confirming that pathological hyperphosphorylation of tau is linked to amyloid-β deposition in this mouse model (Grueninger *et al.*, 2010).

To confirm the effect of immunotherapy on another tau phosphorylation site, phospho-S422 tau was stained on adjacent sections of the hippocampus. Again, the number of CA1 neurons with a somatodendritic accumulation of phospho-S422 tau was significantly reduced in the mAb-11 IgG2a-treated mice compared to control animals ($P = 0.006$) (Fig. 8D and E). Next, to assess the effect on tau misfolding, we performed a staining with the conformation-dependent MC1 antibody. The number of MC1-positive neuronal cell bodies in CA1 hippocampus was significantly decreased in mAb-11 IgG2a-treated mice ($P = 0.0098$).

Altogether, these results indicate that preventive passive immunization using ECT delivery of recombinant mAb-11 IgG2a antibodies in the periphery is an effective approach to chronically deliver therapeutic antibodies, reduce amyloid deposition throughout the brain and mitigate downstream effects on the tau pathology.

Discussion

The implantation of genetically engineered cells within a retrievable subcutaneous device leads to the continuous production of monoclonal antibodies *in vivo*. This technology achieves steady therapeutic monoclonal antibody levels in the plasma, offering an effective alternative to bolus injections for passive immunization against chronic diseases. Peripheral delivery of anti-amyloid-β monoclonal antibody by ECT leads to a significant reduction of amyloid burden in two mouse models of Alzheimer's disease. The effect of the ECT treatment is more pronounced when passive immunization is preventively administered in TauPS2APP mice, most notably decreasing the phospho-tau pathology.

With the recent development of biomarkers to monitor Alzheimer's pathology, it is recognized that a steady increase in cerebral amyloid over the course of decades precedes the appearance of the first cognitive symptoms (reviewed in Sperling *et al.*, 2011). The current consensus therefore suggests applying anti-amyloid-β immunotherapy during this long asymptomatic phase to avoid the downstream consequences of amyloid deposition and to leverage neuroprotective effects. Several preventive clinical trials have been recently initiated for Alzheimer's disease. The Alzheimer's Prevention Initiative (API) and the Dominantly Inherited Alzheimer Network (DIAN) will test antibody candidates in presymptomatic dominant mutation carriers, while the Anti-Amyloid treatment in the Asymptomatic Alzheimer's disease (A4) trial enrols asymptomatic subjects after risk stratification. If individuals with a high risk of developing Alzheimer's disease can be identified using current biomarker candidates, these patients are the most likely to benefit from chronic long-term anti-amyloid-β immunotherapy. However, such a treatment may pose a challenge to healthcare systems, as the production capacity of the antibody and its related cost would become a challenging issue (Skoldunger *et al.*, 2012). Therefore, the development of alternative technologies to chronically administer anti-amyloid-β antibody is an important aspect for therapeutic interventions at preclinical disease stages.

Here, we show that the ECT technology for the peripheral delivery of anti-amyloid-β monoclonal antibodies can significantly reduce cerebral amyloid pathology in two mouse models of Alzheimer's disease. The subcutaneous tissue is a site of implantation easily accessible and therefore well adapted to preventive treatment. It is, however, challenging to reach therapeutic efficacy, as only a small fraction of the produced anti-amyloid-β monoclonal antibodies are expected to cross the blood–brain barrier, although they can next persist in the brain for several months (Wang *et al.*, 2011; Bohrmann *et al.*, 2012). Our results are consistent with previous reports, which have shown that the systemic administration of anti-amyloid-β antibodies can decrease brain amyloid burden in preclinical Alzheimer's disease models (Bard *et al.*, 2000, 2003; DeMattos *et al.*, 2001; Wilcock *et al.*, 2004*a*, *b*; Buttini *et al.*, 2005; Adolfsson *et al.*, 2012).

Remarkably, striking differences exist among therapeutic anti-amyloid-β antibodies in their ability to clear already existing plaques. Soluble amyloid-β species can saturate the small fraction of pan-amyloid-β antibodies entering the CNS and inhibit further target engagement (Demattos *et al.*, 2012). Therefore, antibodies recognizing soluble amyloid-β may fail to bind and clear insoluble amyloid deposits (Das *et al.*, 2001; Racke *et al.*, 2005; Levites *et al.*, 2006; Bohrmann *et al.*, 2012). Furthermore, antibody-amyloid-β complexes are drained towards blood vessels, promoting cerebral amyloid angiopathy (CAA) and subsequent microhaemorrhages. The mAb-11 antibody used in the present study is similar to gantenerumab, which is highly specific for amyloid plaques and reduces amyloid

burden in patients with Alzheimer's disease (Bohrmann *et al.*, 2012; Demattos *et al.*, 2012; Ostrowitzki *et al.*, 2012). We find that the murine IgG2a mAb-11 antibody efficiently enhances the phagocytosis of amyloid-β fibrils by microglial cells. In addition, ECT administration of the mAb-11 $F(ab')_2$ fragment lacking the Fc region fails to recruit microglial cells, and leads only to a trend towards clearance of the amyloid plaques. Therefore, our results suggest a pivotal role for microglial cells in the clearance of amyloid plaques following mAb-11 delivery by ECT. Importantly, we do not find any evidence that this treatment may cause microhaemorrhages in the mouse models used in this study. It remains entirely possible that direct binding to amyloid plaques of a $F(ab')_2$ fragment lacking effector functionality can contribute to therapeutic efficacy, as suggested by previous studies using antibody fragments (Bacskai *et al.*, 2002; Tamura *et al.*, 2005; Wang *et al.*, 2010; Cattepoel *et al.*, 2011). However, compared to IgG2a, the lower plasma levels achieved with $F(ab')_2$ are likely to limit the efficacy of peripheral ECT-mediated immunization. The exact role of the effector domain and its interaction with immune cells expressing Fc receptors, could be determined by comparing the therapeutic effects of a control antibody carrying a mutated Fc portion, similar to a previous study which addressed this question using deglycosylated anti-amyloid-β antibodies (Wilcock *et al.*, 2006*a*; Fuller *et al.*, 2014).

Remarkably, continuous administration of mAb-11 initiated before plaque deposition had a dramatic effect on the amyloid pathology in TauPS2APP mice, underlining the efficacy of preventive anti-amyloid-β treatments. In this mouse model, where tau hyperphosphorylation is enhanced by amyloid-β (Grueninger *et al.*, 2010), the treatment decreases the number of AT8- and phospho-S422-positive neurons in the hippocampus. Furthermore, the number of MC1-positive hippocampal neurons is significantly reduced, which also indicates an effect of anti-amyloid-β immunotherapy on the accumulation of misfolded tau. These results highlight the effect of amyloid-β clearance on other manifestations of the Alzheimer's pathology. In line with these findings, previous studies have shown evidence for a decrease in tau hyperphosphorylation following immunization against amyloid-β, both in animal models and in patients with Alzheimer's disease (Oddo *et al.*, 2004; Wilcock *et al.*, 2009; Boche *et al.*, 2010; Serrano-Pozo *et al.*, 2010; Salloway *et al.*, 2014).

Similar to the subcutaneous injection of recombinant proteins (Schellekens, 2005), ECT implants can elicit significant immune responses against the secreted recombinant antibody. An anti-drug antibody response was detected in half of the mice treated with the mAb-11-releasing devices, in the absence of any anti-CD4 treatment. The glycosylation profile of the mAb-11 synthesized in C2C12 myoblasts is comparable to standard material produced by myeloma or HEK293 cells (Lathuiliere *et al.*, 2014*a*). Although we cannot exclude that local release by ECT leads to antibody aggregation and denaturation, it is unlikely that this mode of administration further contributes to compound immunogenicity. Because the Fab regions of the chimeric recombinant mAb-11 IgG2a contain human CDRs, it remains to be determined whether the ECT-mediated delivery of antibodies fully matched with the host species would trigger an anti-drug antibody response.

Further developments will be needed to scale up this delivery system to humans. The possibility of using a single allogeneic cell source for all intended recipients is a crucial advantage of the ECT technology to standardize monoclonal antibody delivery. However, the development of renewable cell sources of human origin will be essential to ECT application in the clinic. Although the ARPE-19 cell line has been successfully adapted to ECT and used in clinical trials (Dunn *et al.*, 1996; Zhang *et al.*, 2011), the development of human myogenic cells (Negroni *et al.*, 2009) is an attractive alternative that is worth exploring. Based on the PK analysis of recombinant mAb-11 antibody subcutaneously injected in mice (Supplementary material), we estimate that the flat sheet devices chronically release mAb-11 at a rate of 6.8 and 11.8 μg/h, to reach a plasma level of 50 μg/ml in the implanted animals. In humans, injected IgG1 has a longer half-life (21–25 days), with a volume of distribution of ∼100 ml/kg and an estimated clearance of 0.2 ml/h/kg. These values indicate that the predicted antibody exposure in humans, based on the rate of mAb-11 secretion achieved by ECT in mice, would be only 10 to 20-fold lower than the typical regimens based on monthly bolus injection of 1 mg/kg anti-amyloid-β monoclonal antibody. Hence, it is realistic to consider ECT for therapeutic monoclonal antibody delivery in humans, as the flat sheet device could be scaled up to contain higher amounts of cells. Furthermore, recent progress to engineer antibodies for increased penetration into the brain will enable lowering dosing of biotherapeutics to achieve therapeutic efficacy (Bien-Ly *et al.*, 2014; Niewoehner *et al.*, 2014). For some applications, intrathecal implantation could be preferred to chronically deliver monoclonal antibodies directly inside the CNS (Aebischer *et al.*, 1996; Marroquin Belaunzaran *et al.*, 2011).

Overall, ECT provides a novel approach for the local and systemic delivery of recombinant monoclonal antibodies in the CNS. It will expand the possible therapeutic options for immunotherapy against neurodegenerative disorders associated with the accumulation of misfolded proteins, including Alzheimer's and Parkinson's diseases, dementia with Lewy bodies, frontotemporal lobar dementia and amyotrophic lateral sclerosis (Gros-Louis *et al.*, 2010; Bae *et al.*, 2012; Rosenmann, 2013).

Acknowledgements

The authors thank Aline Aebi, Fabienne Pidoux, Vivianne Padrun, Christel Sadeghi and Philippe Colin at EPFL for outstanding technical support, Steffen Cosson and Matthias Lütolf for providing the PEG hydrogel matrix for the

devices. The authors thank Christophe Schweitzer at Roche for technical support to the cloning of the chimeric recombinant mAb-11, Kevin Brady for performing the pharmacokinetic analysis, Kay Stubenrauch for developing mAb-11 detection ELISA, and Hansruedi Loetscher for continuous support to the project. The authors thank Christine Rothe, Margit Urban, Michael Bardroff and Robert Rauchenberger and MorphoSys, Martinsried, Germany for their contributions that led to the identification of mAb-11, as well as P. Davies (Bronx, NY) for providing the MC1 antibody.

Funding

This work was supported by the Swiss Commission for Technology and Innovation (CTI, grant no. 14666.1 PFLS-LS), as well as by F. Hoffmann-La Roche Ltd.

Supplementary material

Supplementary material is available at *Brain* online.

References

Adolfsson O, Pihlgren M, Toni N, Varisco Y, Buccarello AL, Antoniello K, et al. An effector-reduced anti-beta-amyloid (Abeta) antibody with unique abeta binding properties promotes neuroprotection and glial engulfment of Abeta. J Neurosci 2012; 32: 9677–89.

Aebischer P, Schluep M, Deglon N, Joseph JM, Hirt L, Heyd B, et al. Intrathecal delivery of CNTF using encapsulated genetically modified xenogeneic cells in amyotrophic lateral sclerosis patients. Nat Med 1996; 2: 696–9.

Alliot F, Marty MC, Cambier D, Pessac B. A spontaneously immortalized mouse microglial cell line expressing CD4. Brain Res Dev Brain Res 1996; 95: 140–3.

Astolfo A, Arfelli F, Schultke E, James S, Mancini L, Menk RH. A detailed study of gold-nanoparticle loaded cells using X-ray based techniques for cell-tracking applications with single-cell sensitivity. Nanoscale 2013; 5: 3337–45.

Bacskai BJ, Kajdasz ST, McLellan ME, Games D, Seubert P, Schenk D, et al. Non-Fc-mediated mechanisms are involved in clearance of amyloid-beta in vivo by immunotherapy. J Neurosci 2002; 22: 7873–8.

Bae EJ, Lee HJ, Rockenstein E, Ho DH, Park EB, Yang NY, et al. Antibody-aided clearance of extracellular alpha-synuclein prevents cell-to-cell aggregate transmission. J Neurosci 2012; 32: 13454–69.

Bard F, Barbour R, Cannon C, Carretto R, Fox M, Games D, et al. Epitope and isotype specificities of antibodies to beta -amyloid peptide for protection against Alzheimer's disease-like neuropathology. Proc Natl Acad Sci USA 2003; 100: 2023–8.

Bard F, Cannon C, Barbour R, Burke RL, Games D, Grajeda H, et al. Peripherally administered antibodies against amyloid beta-peptide enter the central nervous system and reduce pathology in a mouse model of Alzheimer disease. Nat Med 2000; 6: 916–19.

Bien-Ly N, Yu YJ, Bumbaca D, Elstrott J, Boswell CA, Zhang Y, et al. Transferrin receptor (TfR) trafficking determines brain uptake of TfR antibody affinity variants. J Exp Med 2014; 211: 233–44.

Boche D, Donald J, Love S, Harris S, Neal JW, Holmes C, et al. Reduction of aggregated Tau in neuronal processes but not in the cell bodies after Abeta42 immunisation in Alzheimer's disease. Acta Neuropathol 2010; 120: 13–20.

Bohrmann B, Baumann K, Benz J, Gerber F, Huber W, Knoflach F, et al. Gantenerumab: a novel human anti-Abeta antibody demonstrates sustained cerebral amyloid-beta binding and elicits cell-mediated removal of human amyloid-beta. J Alzheimers Dis 2012; 28: 49–69.

Buttini M, Masliah E, Barbour R, Grajeda H, Motter R, Johnson-Wood K, et al. Beta-amyloid immunotherapy prevents synaptic degeneration in a mouse model of Alzheimer's disease. J Neurosci 2005; 25: 9096–101.

Cattepoel S, Hanenberg M, Kulic L, Nitsch RM. Chronic intranasal treatment with an anti-Abeta(30-42) scFv antibody ameliorates amyloid pathology in a transgenic mouse model of Alzheimer's disease. PLoS ONE 2011; 6: e18296

Charrier S, Stockholm D, Seye K, Opolon P, Taveau M, Gross DA, et al. A lentiviral vector encoding the human Wiskott-Aldrich syndrome protein corrects immune and cytoskeletal defects in WASP knockout mice. Gene Ther 2005; 12: 597–606.

Collin L, Bohrmann B, Gopfert U, Oroszlan-Szovik K, Ozmen L, Gruninger F. Neuronal uptake of tau/pS422 antibody and reduced progression of tau pathology in a mouse model of Alzheimer's disease. Brain 2014; 137: 2834–46.

Das P, Murphy MP, Younkin LH, Younkin SG, Golde TE. Reduced effectiveness of Abeta1-42 immunization in APP transgenic mice with significant amyloid deposition. Neurobiol Aging 2001; 22: 721–7.

DeMattos RB, Bales KR, Cummins DJ, Dodart JC, Paul SM, Holtzman DM. Peripheral anti-A beta antibody alters CNS and plasma A beta clearance and decreases brain A beta burden in a mouse model of Alzheimer's disease. Proc Natl Acad Sci USA 2001; 98: 8850–5.

Demattos RB, Lu J, Tang Y, Racke MM, Delong CA, Tzaferis JA, et al. A plaque-specific antibody clears existing beta-amyloid plaques in Alzheimer's disease mice. Neuron 2012; 76: 908–20.

Doody RS, Thomas RG, Farlow M, Iwatsubo T, Vellas B, Joffe S, et al. Phase 3 trials of solanezumab for mild-to-moderate Alzheimer's disease. N Engl J Med 2014; 370: 311–21.

Dunn KC, Aotaki-Keen AE, Putkey FR, Hjelmeland LM. ARPE-19, a human retinal pigment epithelial cell line with differentiated properties. Exp Eye Res 1996; 62: 155–69.

Ehrbar M, Rizzi SC, Schoenmakers RG, Miguel BS, Hubbell JA, Weber FE, et al. Biomolecular hydrogels formed and degraded via site-specific enzymatic reactions. Biomacromolecules 2007; 8: 3000–7.

Fuller JP, Stavenhagen JB, Teeling JL. New roles for Fc receptors in neurodegeneration-the impact on Immunotherapy for Alzheimer's Disease. Front Neurosci 2014; 8: 235

Geng D, Shankar G, Schantz A, Rajadhyaksha M, Davis H, Wagner C. Validation of immunoassays used to assess immunogenicity to therapeutic monoclonal antibodies. J Pharm Biomed Anal 2005; 39: 364–75.

Goate A, Hardy J. Twenty years of Alzheimer's disease-causing mutations. J Neurochem 2012; 120: 3–8.

Gros-Louis F, Soucy G, Lariviere R, Julien JP. Intracerebroventricular infusion of monoclonal antibody or its derived Fab fragment against misfolded forms of SOD1 mutant delays mortality in a mouse model of ALS. J Neurochem 2010; 113: 1188–99.

Grueninger F, Bohrmann B, Czech C, Ballard TM, Frey JR, Weidensteiner C, et al. Phosphorylation of Tau at S422 is enhanced by Abeta in TauPS2APP triple transgenic mice. Neurobiol Dis 2010; 37: 294–306.

Hardy J, Selkoe DJ. The amyloid hypothesis of Alzheimer's disease: progress and problems on the road to therapeutics. Science 2002; 297: 353–6.

Lathuiliere A, Bohrmann B, Kopetzki E, Schweitzer C, Jacobsen H, Moniatte M, et al. Genetic engineering of cell lines using lentiviral

vectors to achieve antibody secretion following encapsulated implantation. Biomaterials 2014a; 35: 792–802.
Lathuiliere A, Cosson S, Lutolf MP, Schneider BL, Aebischer P. A high-capacity cell macroencapsulation system supporting the long-term survival of genetically engineered allogeneic cells. Biomaterials 2014b; 35: 779–91.
Levites Y, Das P, Price RW, Rochette MJ, Kostura LA, McGowan EM, et al. Anti-Abeta42- and anti-Abeta40-specific mAbs attenuate amyloid deposition in an Alzheimer disease mouse model. J Clin Invest 2006; 116: 193–201.
Marroquin Belaunzaran O, Cordero MI, Setola V, Bianchi S, Galli C, Bouche N, et al. Chronic delivery of antibody fragments using immunoisolated cell implants as a passive vaccination tool. PLoS ONE 2011; 6: e18268
McDonald SA, Marone F, Hintermuller C, Mikuljan G, David C, Pfeiffer F, et al. Advanced phase-contrast imaging using a grating interferometer. J Synchrotron Radiat 2009; 16: 562–72.
Negroni E, Riederer I, Chaouch S, Belicchi M, Razini P, Di Santo J, et al. In vivo myogenic potential of human CD133 + muscle-derived stem cells: a quantitative study. Mol Ther 2009; 17: 1771–8.
Niewoehner J, Bohrmann B, Collin L, Urich E, Sade H, Maier P, et al. Increased brain penetration and potency of a therapeutic antibody using a monovalent molecular shuttle. Neuron 2014; 81: 49–60.
Oakley H, Cole SL, Logan S, Maus E, Shao P, Craft J, et al. Intraneuronal beta-amyloid aggregates, neurodegeneration, and neuron loss in transgenic mice with five familial Alzheimer's disease mutations: potential factors in amyloid plaque formation. J Neurosci 2006; 26: 10129–40
Oddo S, Billings L, Kesslak JP, Cribbs DH, LaFerla FM. Abeta immunotherapy leads to clearance of early, but not late, hyperphosphorylated tau aggregates via the proteasome. Neuron 2004; 43: 321–32.
Ostrowitzki S, Deptula D, Thurfjell L, Barkhof F, Bohrmann B, Brooks DJ, et al. Mechanism of amyloid removal in patients with Alzheimer disease treated with gantenerumab. Arch Neurol 2012; 69: 198–207.
Pinzer BR, Cacquevel M, Modregger P, McDonald SA, Bensadoun JC, Thuering T, et al. Imaging brain amyloid deposition using grating--based differential phase contrast tomography. Neuroimage 2012; 61: 1336–46.
Racke MM, Boone LI, Hepburn DL, Parsadainian M, Bryan MT, Ness DK, et al. Exacerbation of cerebral amyloid angiopathy-associated microhemorrhage in amyloid precursor protein transgenic mice by immunotherapy is dependent on antibody recognition of deposited forms of amyloid beta. J Neurosci 2005; 25: 629–36.
Rauchenberger R, Borges E, Thomassen-Wolf E, Rom E, Adar R, Yaniv Y, et al. Human combinatorial Fab library yielding specific and functional antibodies against the human fibroblast growth factor receptor 3. J Biol Chem 2003; 278: 38194–205.
Rosenmann H. Immunotherapy for targeting tau pathology in Alzheimer's disease and tauopathies. Curr Alzheimer Res 2013; 10: 217–28.
Salloway S, Sperling R, Fox NC, Blennow K, Klunk W, Raskind M, et al. Two phase 3 trials of bapineuzumab in mild-to-moderate Alzheimer's disease. New Eng J Med 2014; 370: 322–33.
Schellekens H. Factors influencing the immunogenicity of therapeutic proteins. Nephrol Dial Transplant 2005; 20: vi3–9.
Serrano-Pozo A, William CM, Ferrer I, Uro-Coste E, Delisle MB, Maurage CA, et al. Beneficial effect of human anti-amyloid- active immunization on neurite morphology and tau pathology. Brain 2010; 133: 1312–27.
Shankar G, Devanarayan V, Amaravadi L, Barrett YC, Bowsher R, Finco-Kent D, et al. Recommendations for the validation of immunoassays used for detection of host antibodies against biotechnology products. J Pharm Biomed Anal 2008; 48: 1267–81.
Skoldunger A, Wimo A, Johnell K. Net costs of dementia in Sweden - an incidence based 10 year simulation study. Int J Geriatr Psychiatry 2012; 27: 1112–17.
Sperling R, Salloway S, Brooks DJ, Tampieri D, Barakos J, Fox NC, et al. Amyloid-related imaging abnormalities in patients with Alzheimer's disease treated with bapineuzumab: a retrospective analysis. Lancet Neurol 2012; 11: 241–9.
Sperling RA, Aisen PS, Beckett LA, Bennett DA, Craft S, Fagan AM, et al. Toward defining the preclinical stages of Alzheimer's disease: recommendations from the National Institute on Aging-Alzheimer's Association workgroups on diagnostic guidelines for Alzheimer's disease. Alzheimers Dement 2011; 7: 280–92.
Tabrizi M, Bornstein GG, Suria H. Biodistribution mechanisms of therapeutic monoclonal antibodies in health and disease. AAPS J 2010; 12: 33–43.
Tamura Y, Hamajima K, Matsui K, Yanoma S, Narita M, Tajima N, et al. The F(ab)'2 fragment of an Abeta-specific monoclonal antibody reduces Abeta deposits in the brain. Neurobiol Dis 2005; 20: 541–9.
Wang A, Das P, Switzer RC, 3rd, Golde TE, Jankowsky JL. Robust amyloid clearance in a mouse model of Alzheimer's disease provides novel insights into the mechanism of amyloid-beta immunotherapy. J Neurosci 2011; 31: 4124–36.
Wang W, Wang EQ, Balthasar JP. Monoclonal antibody pharmacokinetics and pharmacodynamics. Clin Pharmacol Ther 2008; 84: 548–58.
Wang YJ, Gao CY, Yang M, Liu XH, Sun Y, Pollard A, et al. Intramuscular delivery of a single chain antibody gene prevents brain Abeta deposition and cognitive impairment in a mouse model of Alzheimer's disease. Brain Behav Immun 2010; 24: 1281–93.
Webster SD, Galvan MD, Ferran E, Garzon-Rodriguez W, Glabe CG, Tenner AJ. Antibody-mediated phagocytosis of the amyloid beta-peptide in microglia is differentially modulated by C1q. J Immunol 2001; 166: 7496–503.
Weitkamp T, Diaz A, David C, Pfeiffer F, Stampanoni M, Cloetens P, et al. X-ray phase imaging with a grating interferometer. Opt Express 2005; 13: 6296–304.
Wilcock DM, Alamed J, Gottschall PE, Grimm J, Rosenthal A, Pons J, et al. Deglycosylated anti-amyloid-beta antibodies eliminate cognitive deficits and reduce parenchymal amyloid with minimal vascular consequences in aged amyloid precursor protein transgenic mice. J Neurosci 2006a; 26: 5340–6.
Wilcock DM, Gharkholonarehe N, Van Nostrand WE, Davis J, Vitek MP, Colton CA. Amyloid reduction by amyloid-beta vaccination also reduces mouse tau pathology and protects from neuron loss in two mouse models of Alzheimer's disease. J Neurosci 2009; 29: 7957–65.
Wilcock DM, Gordon MN, Morgan D. Quantification of cerebral amyloid angiopathy and parenchymal amyloid plaques with Congo red histochemical stain. Nat Protoc 2006b; 1: 1591–5.
Wilcock DM, Rojiani A, Rosenthal A, Levkowitz G, Subbarao S, Alamed J, et al. Passive amyloid immunotherapy clears amyloid and transiently activates microglia in a transgenic mouse model of amyloid deposition. J Neurosci 2004a; 24: 6144–51.
Wilcock DM, Rojiani A, Rosenthal A, Subbarao S, Freeman MJ, Gordon MN, et al. Passive immunotherapy against Abeta in aged APP-transgenic mice reverses cognitive deficits and depletes parenchymal amyloid deposits in spite of increased vascular amyloid and microhemorrhage. J Neuroinflammation 2004b; 1: 24.
Yaffe D, Saxel O. Serial passaging and differentiation of myogenic cells isolated from dystrophic mouse muscle. Nature 1977; 270: 725–7.
Zhang K, Hopkins JJ, Heier JS, Birch DG, Halperin LS, Albini TA, et al. Ciliary neurotrophic factor delivered by encapsulated cell intraocular implants for treatment of geographic atrophy in age-related macular degeneration. Proc Natl Acad Sci USA 2011; 108: 6241–5.
Zufferey R. Production of lentiviral vectors. Curr Top Microbiol Immunol 2002; 261: 107–21.